Chapter 2
Strategies for the Fabrication of Wrinkled Polymer Surfaces

C. M. González-Henríquez, M. A. Sarabia Vallejos, and Juan Rodríguez-Hernández

2.1 Introduction

A large amount of work has been carried out in the fabrication of different surface patterns based on surface instabilities. In particular, the wrinkled formation is one of the most extensively explored strategies to produce surface micro- and submicrometer scale structures. In order to organize the extensive literature reported in this area, we propose the classification of the different strategies first taking into account the film structure distinguishing three different situations: layered films, gradient, and homogeneous. Thus, this chapter is organized as follows. First, we will briefly describe the possible film structures to produce wrinkled structures. Second, we will, as a function of the film structure, discuss the different methodologies and the stimuli employed to induce buckling and thus produce wrinkled surface morphologies.

C. M. González-Henríquez
Departamento de Química, Facultad de Ciencias Naturales, Matemáticas y del Medio Ambiente, Universidad Tecnológica Metropolitana, Santiago, Chile

Programa Institucional de Fomento a la Investigación, Desarrollo e Innovación, Universidad Tecnológica Metropolitana, San Joaquín, Santiago, Chile

M. A. Sarabia Vallejos
Escuela de Ingeniería, Departamento de Ingeniería Estructural y Geotecnia, Pontificia Universidad Católica de Chile, Santiago, Chile

Instituto de Ingeniería Biológica y Médica, Santiago, Chile

J. Rodríguez-Hernández (✉)
Departamento de Química Macromolecular Aplicada, Polymer Functionalization Group, Instituto de Ciencia y Tecnología de Polímeros-Consejo Superior de Investigaciones Científicas (ICTP-CSIC), Madrid, Spain
e-mail: jrodriguez@ictp.csic.es

C. M. González-Henríquez, J. Rodríguez-Hernández (eds.), *Wrinkled Polymer Surfaces*, https://doi.org/10.1007/978-3-030-05123-5_2

2.1.1 Films Structures of Wrinkled Surfaces

Wrinkle formation of polymer surfaces can be obtained using a large variety of different strategies [1–6] that can, otherwise, be divided and organized into three categories as a function of the structure of the precursor film. We can thus distinguish between (1) films formed by distinct layers (two or more), (2) homogeneous films, and (3) depth-wise gradient films formed by a gradual variation of the chemical/physical/mechanical properties from the surface to the bulk (Fig. 2.1).

Inside of each family, we will, in turn, subdivide into different groups taking into account the stimulus employed to induce wrinkle formation.

2.2 Layered Systems Composed of Layers with Dissimilar Mechanical Properties

Layered films are formed by two or more polymer or hybrid polymer/metal layers with, unlike mechanical properties. In order to describe the alternatives to obtain wrinkles from layered films, we will first describe the materials typically employed as substrates and as top layers including the methodologies used to achieve a rigid layer on the top of an elastic foundation. Then, we will classify the approaches reported to produce surface wrinkles based on the type of force applied to modify the form of the elastic foundation inducing the buckling of the rigid top layer.

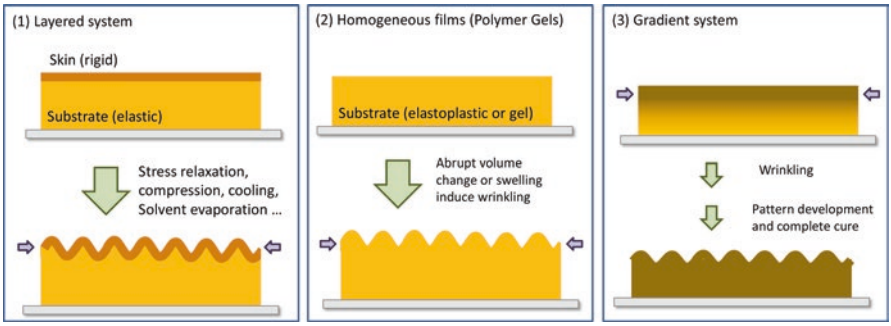

Fig. 2.1 Film structures capable of forming wrinkles: (1) Layered film structure composed of an elastic substrate and a rigid skin, (2) homogeneous films (typically homogeneously cross-linked hydrogels), and (3) gradient film with variable mechanical properties as a function of the depth. (Reproduced with permission from ref. [7])

2.2.1 Bilayered Systems: Structure and Materials

2.2.1.1 Types of Substrates in Bilayered Systems

Whereas initial works have been mainly focused on the use of elastic substrates, typically PDMS, in view of enlarging the potential applications of wrinkled surfaces, other substrates have been equally proposed to produce wrinkled patterned structures. As a result, the substrate or film can be:

(a) *Liquid substrates*

Huang et al. [8] employed circular pieces of PS film detached from the substrate supported on deionized water. Later Vella [9] used the same system to explain the origin of the wrinkling of such membranes observed by Holmes et al. [10] employed a thin polymer film, either polydimethylsiloxane (PDMS) or polystyrene (PS), which is prepared via spin coating a polymer solution onto a clean silicon wafer. A circular film of radius L = 17:5 mm is floated off the wafer onto the surface of the water. As depicted in Fig. 2.2, they found that the wrinkle wavelength is dictated by a balance of material properties and geometry, most directly the thickness of the

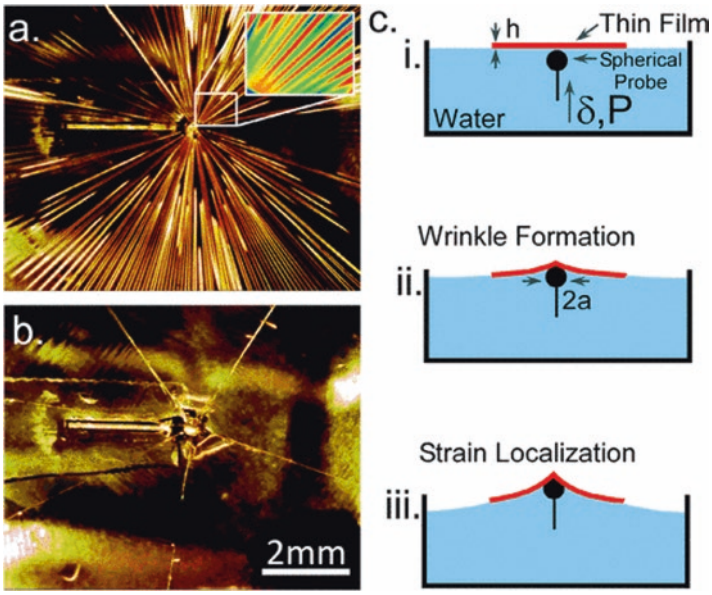

Fig. 2.2 (**a**) Wrinkles on a thin film floating on water lifted by a spherical probe (inset: image via optical profilometry). (**b**) As the vertical displacement of the probe increases, the wrinkles localize into sharp folds. (**c**) Schematic of the experimental setup, where (i) depicts the axisymmetric thin film floating on water, (ii) the formation of wrinkles as the probe displaces the film vertically, and (iii) the critical displacement at which wrinkles collapse into folds. (Reproduced with permission from ref. [10])

draping film. At a critical strain, the stress in the film will localize, causing hundreds of wrinkles to collapse into several discrete folds.

Finally, another interesting example was reported by Pocivavsek et al. [11]. They employed a polyester of the top or either Millipore water or a soft gel. They explore the wrinkle formation and also the morphological transitions and found that a wrinkle-to-fold transition (Fig. 2.3A) takes place when the polyester sheet is lying on top of the water. However, the liquid substrate is not required for the transition to occur since (Fig. 2.3B) a similar evolution of the surface was observed with the polyester adhered to a soft gel. Moreover, smooth wrinkling (a in Fig. 2.3B) develops

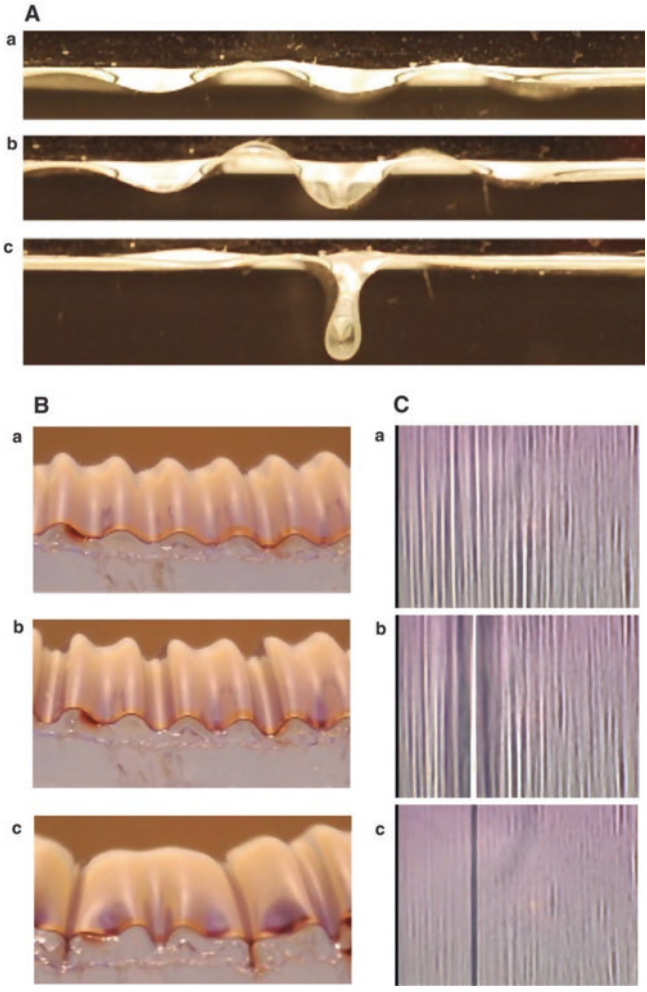

Fig. 2.3 (**A**) Polyester film on water, (**B**) polyester film on gel substrate, and (**C**) trilayer of colloidal gold nanoparticles on water. (Reproduced with permission from ref. [11])

to unstable (b in Fig. 2.3B) and can potentially produce several folds relaxing the rest of the surface (c in Fig. 2.3B).

(b) *Viscous liquids as substrates*

Pioneer theoretical studies compared to experimental data about wrinkle formation on viscous liquids were carried out by Suo et al. [12, 13]. According to Suo et al., compressively stressed elastic films on finite-thickness viscous substrates may experience a buckling instability and, as a result, release stresses that may finally alter the planarity of the film. They carried out a linear stability analysis to assess the onset and maximally unstable mode of this buckling instability as a function of three main parameters, i.e., the thickness of the viscous layer, misfit strain, and viscosity. They found that the onset of the buckling instability of the film on a glass layer is the same as that retrieved in a compressively stressed free-standing film. However, the maximally unstable wavelength increases as the glass layer thickness increases.

More recently, Huang and coworkers [14] explored the buckling occurring on thin elastic films floating on a viscous liquid layer, in turn, supported on a pre-stretched rubber sheet (Fig. 2.4). Upon release of the stretching applied in the rubber, a viscous stress is induced in the liquid which, according to Huang et al., produced, in turn, a compressive stress in the elastic film and finally produced the buckling of the film. In contrast to previous studies on the wrinkling of floating films, the authors evidenced that the buckling process was dominated by viscous effects, whereas gravitational effects are negligible. The experimental work carried out using elastic polymer films and viscous polymer liquids evidenced trends that are qualitatively consistent with the predictions calculated using theoretical approaches. However, quantitatively, the experimentally measured wrinkle wavelengths were larger than predicted by the models.

(c) *Viscoelastic substrates*

Viscoelastic substrates and, in particular, polymers are probably the most explored type of substrates to produce surface wrinkling. Using these substrates, previous theoretical [15–17] and experimental [18–21] studies evidenced that under isothermal conditions, the time evolution of both the wrinkle amplitude and wavelength is directly connected to the viscoelastic response of the polymer film at the

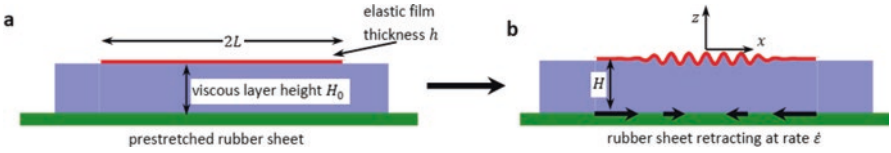

Fig. 2.4 (**a**) Initially flat film floating on a fluid layer, covering a pre-stretched rubber sheet. (**b**) Film wrinkles when the rubber sheet is unstretched at a controlled rate. (Reproduced with permission from ref. [14])

annealing temperature. The annealing temperatures employed are typically near or slightly above the glass transition temperature of the polymer.

Chan et al. [22] employed the thermal-induced surface wrinkling to determine both the rubbery modulus and shear viscosity of polystyrene (PS) film depending on the annealing temperature. For this purpose, as depicted in Fig. 2.5, the authors employed surface laser-light scattering (SLS) to determine the wrinkled surface in real time. They monitored the changes in surface morphology as a function of annealing time at fixed annealing temperatures. Finally, the results obtained were compared to theoretical models that permitted the calculation of the viscoelastic properties of the PS thin film.

Im and Huang [16] reported a theoretical model to explain the wrinkle evolution in a bilayer thin film consisting of an elastic layer and a viscoelastic layer. They employed a thin-layer approximation for the viscoelastic layer. Moreover, the elastic layer subjected to a compressive residual stress was modeled by the nonlinear von Karman plate theory. The authors reported three stages of the wrinkle evolution and are identified as follows: the initial growth of the fastest-growing mode, intermediate growth with mode transition, and, finally, an equilibrium wrinkle state.

Finally, another illustrative example was reported by Hoo et al. [23]. As depicted in Fig. 2.6, they described the evolution of the wrinkle morphologies in a thin bilayer film of an elastic metal on a viscoelastic polymer. As explained by Hoo et al., a transition of initial island-like patterns (annealing time of several minutes) to a wrinkled structure occurs without a change in the wavelength. Moreover, the initially wrinkled structure is transformed into a mountainous topography in the late

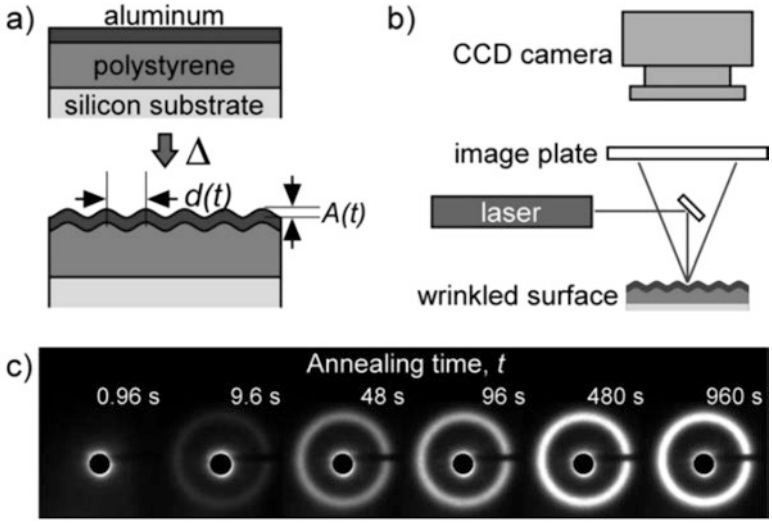

Fig. 2.5 (**a**) Schematic of thermal wrinkling approach to measuring the rubbery modulus and viscosity of a confined PS thin film. (**b**) Schematic of the SLS experimental setup. (**c**) Representative time-evolved scattering patterning as captured by the SLS at 125 °C. (Reproduced with permission from ref. [22])

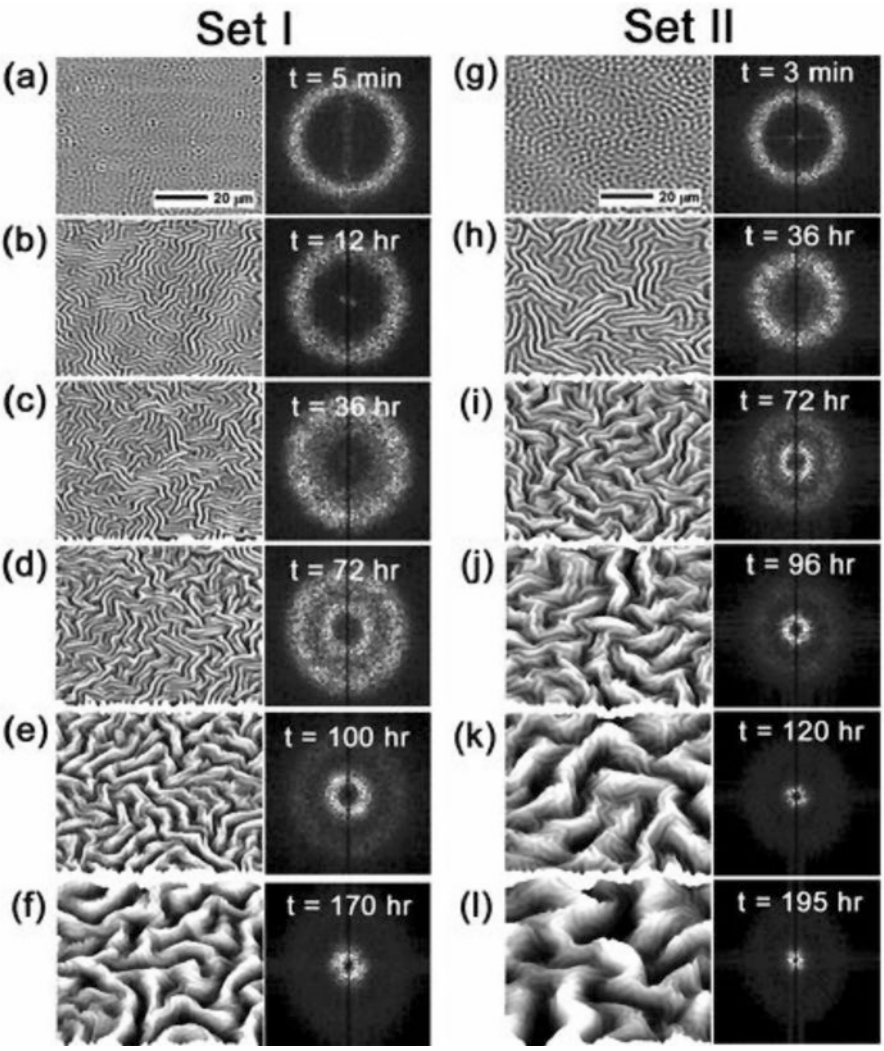

Fig. 2.6 AFM images of the temporal evolution of stress-driven surface wavy patterns. Set I (**a**)–(**f**) is for smaller waves that result in a thin metal layer (40 nm) and a relatively thin polymer layer (350 nm), and set II (**g**)–(**l**) is for larger waves that result when the polymer layer is made thicker (580 nm). (**a**) Set I data after 3 min. (**b**) Set I data after 12 h. (**c**) Set I data after 36 h. (**d**) Set I data after 72 h. (**e**) Set I data after 100 h. (**f**) Set I data after 170 h. (**g**) Set II data after 3 min. (**h**) Set II data after 36 h. (**i**) Set II data after 72 h. (**j**) Set II data after 96 h. (**k**) Set II data after 120 h. (**l**) Set II data after 195 h. (Reproduced with permission from ref. [23])

stages that goes along with an increase in the length scale. This change in the wrinkle wavelength can be associated with the relaxation of the confined polymer that results in a transition from elastic- to viscous-like behavior, induces wave coarsening and macroscopic roughening [23].

(d) *Substrates capable of yielding or softening upon increasing temperature*

Examples of the use of substrates capable of yielding or softening are scarce neither from a theoretical nor from an experimental point of view. One of few examples was reported by Srinivasan et al. [24] who presented a theoretical analysis of the wrinkling processes where irreversible deformation occurs in the foundation. The proposed method was applicable to the analysis of foundations with elastic–damage response and to foundations with an elastoplastic response.

Another interesting example was recently reported by El Haitami et al. [25]. As depicted in Fig. 2.7, the bilayer model comprises a rubber chemically modified at the surface (micrometric depth) to increase the glass transition temperature above room temperature. To produce the surface wrinkles, the authors took advantage of the very slow glassy dynamics of the modified layer. The methodology employed to induce wrinkle formation is based on the difference in the glass transition temperature between the unmodified rubber $T_{g,R}$ and that of the modified layer $T_{g,layer}$ in which the system consists of a glassy layer on top of a rubber substrate. As a result, when the system is heated to above $T_{g,layer}$ (step 1), the system is completely rubbery and can be easily stretched (step 2). In this situation, the modified layer can be

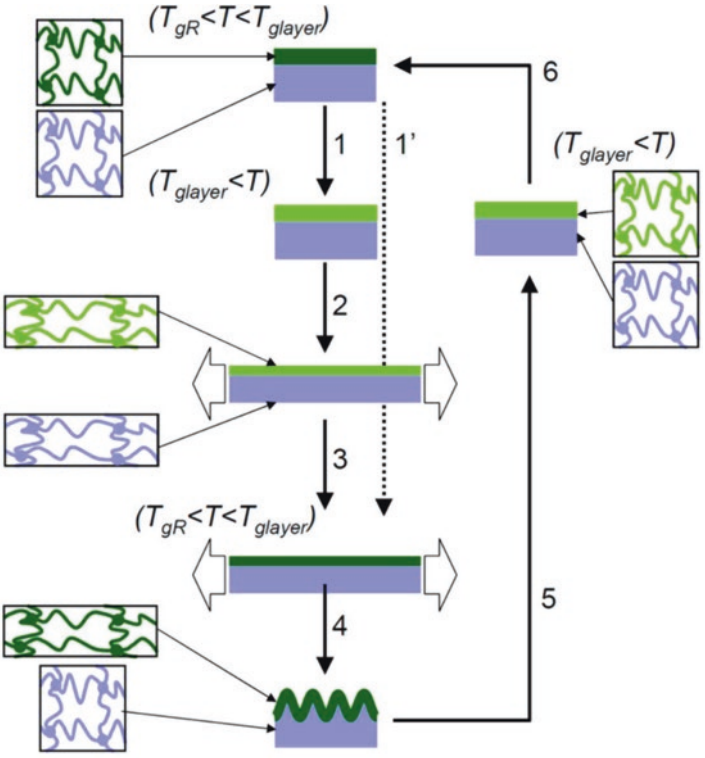

Fig. 2.7 Schematic representation of the proposed wrinkling-unwrinkling approach. (Reproduced with permission from ref. [25])

frozen upon cooling between $T_{g,R}$ and $T_{g,layer}$ maintaining the deformation (step 3). Allowing the unmodified rubber substrate to recover elastically, stable wrinkles were produced (step 4). More interestingly, the wrinkles formed and stable at temperatures below the $T_{g,layer}$ can be erased by heating the system again to above $T_{g,layer}$ (step 5). Since no stretching is applied, the deformed network returns to thermodynamic equilibrium (step 6).

2.2.1.2 Top Layers

The different strategies proposed to obtain a rigid top layer can be grouped into two main approaches. On the one hand, either the substrate is exposed to physical or chemical treatments that change the surface mechanical properties of the substrate (i.e., oxidation of PDMS to produce rigid silica) or the substrate is coated with a rigid film coating (polymeric or metallic).

(a) *Formation of a rigid surface by surface treatments*

A stiff top layer has been achieved, for instance, by *direct oxidation* (UV-ozone or plasma treatments) of the polymer film using an elastic foundation such as PDMS [26–30]. Depending on the oxidation method and also the experimental conditions employed, nano- or microwrinkled surface structures have been obtained (from 150 nm to several hundreds of microns). However, the chemical composition is limited to particular oxides resulting in surface treatments. In addition, the different mechanical resistance of the layer deposited in comparison to the bulk may also introduce additional limitations in the lifetime of the wrinkles since folding and finally cracking can be observed on the surface formed.

Alternative surface treatments include the *reactive ion etching* that using fluorinated gases has been employed to treat polystyrene (PS). This approach permits upon heating the fabrication of wrinkles with precise wavelengths from micrometer down to few nanometers [31]. Finally, it is worth mentioning that *ultraviolet* light [32, 33] or *ion beam* [34] treatments of a pre-stretched substrate can also be employed to increase the stiffness of the skin layer.

(b) *Formation of a rigid top layer by metallic or polymeric thin film deposition*

The second group of strategies to create a bilayer system with layers having different mechanical properties involves the surface coating with a polymeric or even metallic thin layer. This coating is carried out either upon during thermal expansion or mechanical stretching/compression [35, 36]. Pioneer reports by Bowden et al. and Yoo et al. used the evaporation of aluminum that forms the rigid layer on a flexible substrate [35, 37–40]. For instance, the metal can be deposited on the thermally expanded PDMS layer (high temperature) that, upon cooling, will contract and generate a large stress that finally produced the surface wrinkles in the metallic layer. Other works carried out by Fu et al. and Vandeparre et al. resort to different metals such as gold [28] or titanium [41], respectively.

Not only metals but also polymers have been deposited as thin films on top of a substrate to form the bilayer skin or just employed to form the foundation. As has been already mentioned, it is crucial that the polymer employed has a clear difference in stiffness in comparison with the second component of the bilayer system. The most extended alternative involves the deposition of the film by transferring the polymeric films prepared on silicon wafers onto either a compressed or a pre-strained support or by spin coating [42]. Polymers employed for the fabrication of these bilayered structures include homopolymers, such as polystyrene [43] and polypyrrole [44]; more recently, other systems including the fabrication of plastic-rubber composites [45] or the elaboration of bilayers comprising a fluoropolymer (CF_x) skin layer deposited on PDMS [46] soft skin have been equally reported.

Some authors substituted the polymer thin layer by polyelectrolyte multilayers (PEM) usually obtained by the layer-by-layer (LbL) methodology. LbL is carried out by alternating the deposition of positively and negatively charged polyelectrolytes from aqueous solution. This strategy allowed simultaneously to fabricate thin films with controlled composition and thickness [47–50]. For instance, an illustrative example was carried out by Lu et al. that reported the preparation of different multilayer films and found that poly(allylamine hydrochloride)–poly(sodium 4-styrene sulfonate) (PAH–PSS) formed particularly stable wrinkled multilayer films [51].

2.3 Classification of the Wrinkling Mechanisms as a Function of the Stimulus Employed to Induce Surface Buckling

As has been already anticipated in the previous section, wrinkling is usually achieved upon relaxation of a particular stress previously applied. While this is true, the nature of the stress applied to the foundation prior to surface modification can be significantly different:

(a) *Wrinkle formation in response to thermal variations.*

The principle of wrinkle formation due to thermal variations relies on the different expansion coefficients between the top layer and the foundation. More precisely, wrinkles are spontaneously formed due when the stress applied (created either upon heating or cooling) exceeds a critical value particular for each system as a result of the mismatch of thermal expansion coefficient between the substrate and the capping layer. During heating of the substrate, expansion occurs. In an expanded state, either the substrate is treated by using a physical process [22] or polymer/metal is deposited onto the substrate [35, 52]. Finally, upon cooling of the bilayered system, a compressive stress is created in the stiff surface layer that provokes the surface buckling and finally forms wrinkles that remain unaffected when the sample is cooled down [53]. Alternatively, other authors reported the wrinkle formation upon

heating. Illustrative examples of the latter have been reported by Bowden that reported the formation of wrinkled surfaces upon heating using bilayers composed of Al/polystyrene (PS) [26] or the system reported by Huntington based on polystyrene and treated with reactive ion etching [31].

While temperature is a key variable, there are many other variables that can affect the wrinkling such as experimental heating conditions and time, the molecular weight of the polymer, polymer film thickness, or even the cross-linking level of the polymer employed. For instance, in the same work, Yoo and Lee [21] explored the temporal evolution of an elastic wrinkling known as spinodal wrinkling (Fig. 2.8). The authors used a thick film (300–600 nm) of high molecular weight PS as substrate and an Al film (30–60 nm) as the top layer. The wrinkles were produced at 140 °C, which is around 25 °C higher than T_g of the PS. Two distinct transitions in the evolution of the wrinkling morphology can be observed in Fig. 2.8. On the one hand, the transition from an island-like pattern to a labyrinthine pattern is apparent in going from Fig. 2.8a–e. On the other hand, the second transition occurs at longer annealing times and is evidenced by the appearance of a second wave (Fig. 2.8f–h).

More interestingly, the same authors were able to present the different wrinkling regimes. The defined three types of wrinkling were defined by the thermomechanical behavior of the polymer, by strain saturation and bilayer pinning. The morphological diagram as a function of the molecular weight of the polymer employed, the film thickness as well as the processing temperature is depicted in Fig. 2.9. When a high molecular weight is employed (Fig. 2.9a), a remembered elastic response of polymer observed even above the glass transition temperature delivers an elastic contribution in the course of the wrinkle formation. This finally leads to various

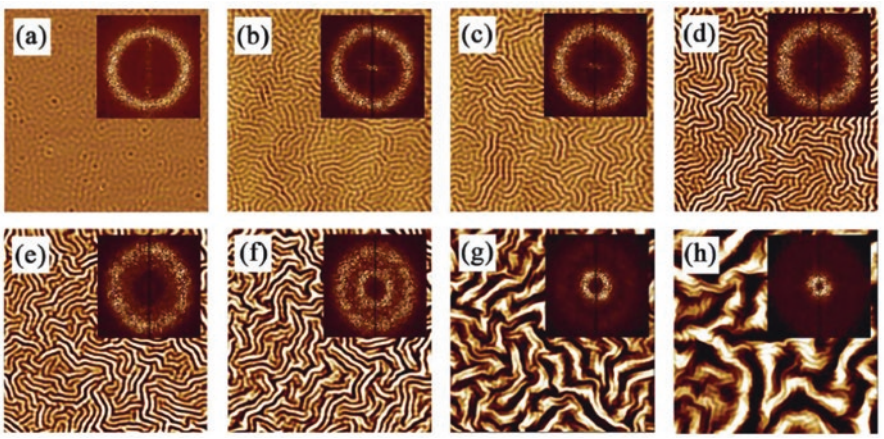

Fig. 2.8 AFM images (80 μm × 80 μm) of the temporal evolution of wrinkled surfaces (40-nm-thick metal layer/350-nm-thick high molecular weight polymer layer/annealing at 140 °C). The insets depict the fast Fourier transform (FFT) images for given patterns: (**a**) after 3 min; (**b**) after 20 min; (**c**) after 3 h; (**d**) after 12 h; (**e**) after 36 h; (**f**) after 72 h; (**g**) after 100 h; (**h**) after 170 h. (Reproduced with permission from ref. [21])

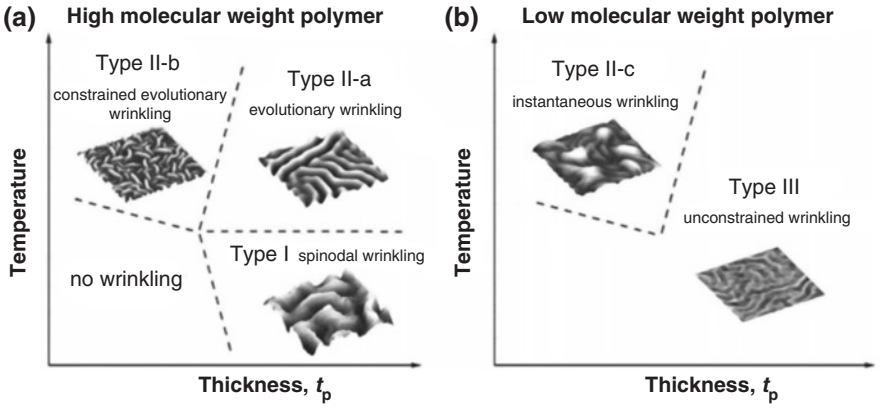

Fig. 2.9 Illustrative wrinkled morphologies observed for the bilayer films as a function of the thickness and annealing temperature. Typical evolutional characteristics are determined by elastic wrinkling (type I) or viscous wrinkling (types II and III). Insets are three-dimensional AFM images for the final morphology of each wrinkling regime. (**a**) High molecular weight polymer layer. (**b**) Low molecular weight polymer layer. (Reproduced with permission from ref. [21])

wrinkling morphologies. In the case of low molecular weight (Fig. 2.9b) polymers, the polymer substrate displays an entirely viscous behavior. This finally favors lower frequency mode and finally approaches an infinite wavelength wrinkle.

Thermal wrinkling on polymer/metal bilayer systems supported on a rigid substrate usually leads to random wrinkles on the surface caused by the compressive stress resulting from thermal annealing (Fig. 2.10a). However, the use of microstructured molds can modify the random organization and produce anisotropic wrinkling [20, 38, 54]. In order to induce the physical confinement effect, Yoo et al. [54, 55] employed a patterned polydimethylsiloxane (PDMS) mold which was placed on top of the metal/polymer bilayer surface prior to heating as depicted in Fig. 2.10. PDMS creates a solid conformal contact with the underlying metal surface, which provokes, in turn, that the edges of the line-and-space pattern act as nodes. As shown in Fig. 2.10b, the selected mold patterns are periodic squares with variable size and period. Interestingly, the resulting self-organized surface structure varied from a simple checkerboard to a more complicated pattern as the pattern period increased from 3 to 10 μm. According to the authors, this is the result of the interactions of the wave generated in the wrinkles with the mold pattern wave or the pattern periodicity.

A similar concept was employed by Kwon et al. [38]. This group reported the preparation of a microstructured polystyrene (PS) layer fabricated by spin coating on a cleaned silicon substrate and then applying capillary force lithography. Thin aluminum films were deposited onto the microstructured PS layer. Finally, upon isothermal annealing, wrinkled structured were produced.

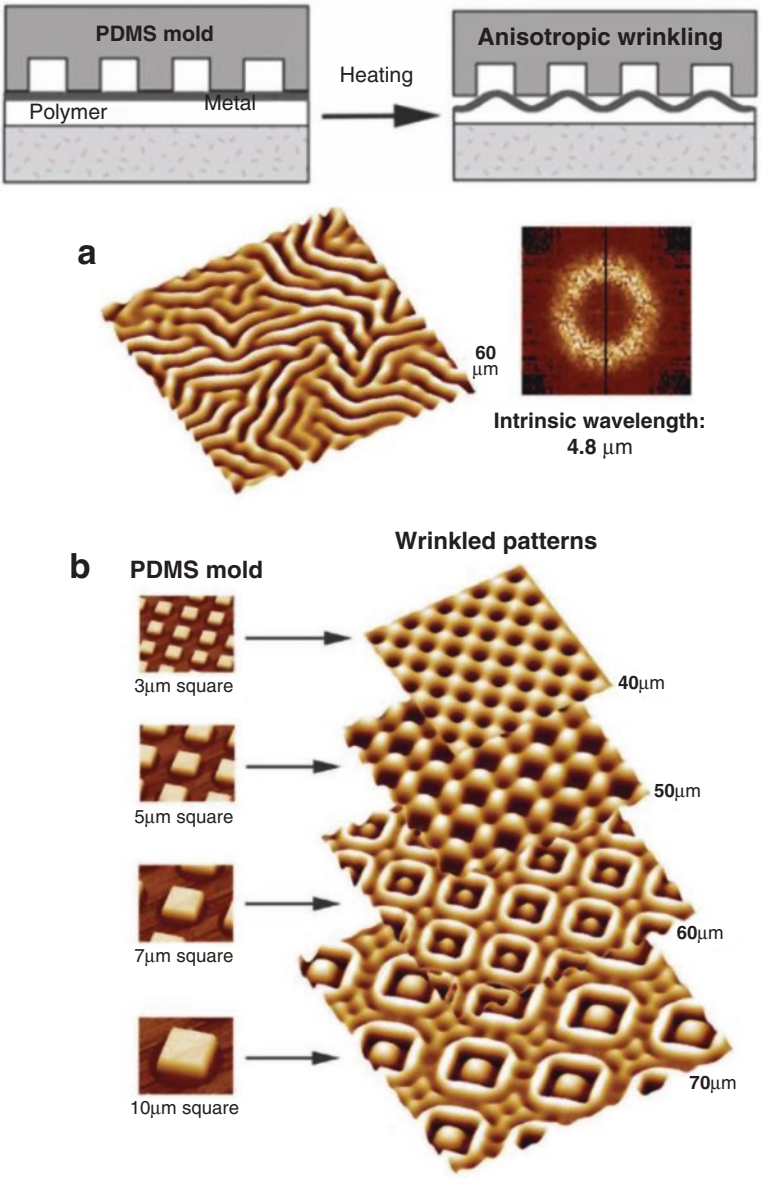

Fig. 2.10 Top: Schematic diagram of the procedure involved in the self-organized anisotropic wrinkling. Down: (**a**) AFM micrographs of the isotropic winkles that result from the bilayer consisting of an 80-nm-thick metal layer (*t*m) and a 600-nm-thick polymer layer (*t*p). (**b**) AFM micrographs of self-organized wrinkle structures obtained through confinement-induced anisotropic wrinkling over the surface used in part a: (top to bottom) checkerboard pattern (3 μm period of the rectangular mold pattern), woven fabric array pattern (5 μm period), encircled dot array pattern (7 μm period), and encircled dot array separated by a tetrapod pattern (10 μm period). (Reproduced with permission from refs. [54, 55])

(b) *Wrinkles formed by mechanical stretching/compression.*

Wrinkles can be also produced by taking advantage of the elastic mechanical properties of a polymer substrate. In general, the strategy involves a uniaxial strain followed by film deposition. Finally, upon stress relaxation, wrinkles are formed at the surface of the elastic foundation. The out-of-plane deformation and thus the formation of the surface wrinkles is the direct consequence of the disparity in Young's modulus between the rigid top layer (E~GPa) and the polymeric substrate (E~MPa). Whereas the wrinkles created by temperature variations are typically random in nature, wrinkles obtained by mechanical stretching/compression are aligned orthogonally to the axis of the deformation. This feature together with the possibility to precisely control the wrinkles dimensions has made of this strategy one of the most extensively employed [56–61].

An illustrative example was reported by Efimenko et al. [62]. They demonstrated that the homogeneity of the buckle morphology depends on the strain removal rate. While the buckle period remains constant, stretched and UVO-modified specimens released at a fast rate (i.e., where the strain has been abruptly removed) usually present a larger number of defects (Fig. 2.11a). However, by decreasing the strain removal rate, the number of defects decreases accordingly. For instance, Fig. 2.11b and c depict optical microscopy images from samples whose strain removal rates

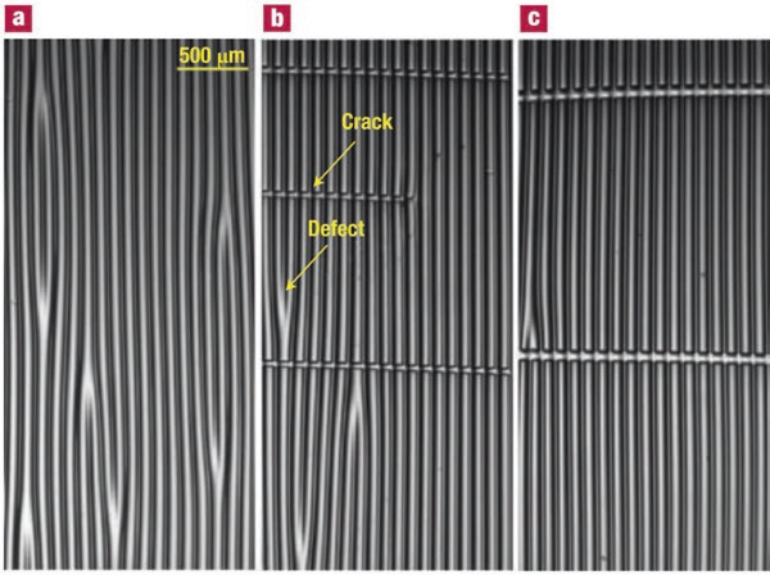

Fig. 2.11 Optical microscopy images were taken in the transmission mode. Samples prepared by stretching PDMS sheets by $\Delta = 50\%$, exposing them to UVO for 60 min and releasing the strain: (**a**), instantaneously and (**b**, **c**) with the strain release rate of ~900 (**b**) and ~58 μm min–1 (**c**). (Reproduced with permission from ref. [62])

were ~900 μm min^{-1} and present ~0.47 defects per mm^2 and ~58 μm min^{-1} with ~0.15 defects per mm^2.

In contrast to the above-depicted methodology that resort to an initial pre-stretching step to produce the surface wrinkles, Ohzono and Shimomura explored the formation of ordered microwrinkled patterns by using a compressive strain [63, 64]. By using this strategy, complex wrinkle stripe patterns composed of convex and concave parts with an almost constant wavelength were ordered in the strain direction. Moreover, the wrinkles disappeared upon stress relaxation.

In general, either stretching or compression has been carried out in one single direction, thus leading to one-dimensional wrinkles. However, several other groups explored the possibility to stretch in different directions. An illustrative example of this alternative was reported by Chun and Yang [65]. The authors report the formation of various submicron wrinkle patterns and their transition from one-dimensional (1D) ripples to two-dimensional (2D) herringbone structures on polydimethylsiloxane films (Fig. 2.12). Using mechanical forces, they can separately control the amount and the timing of strain applied to the substrate on both planar directions either simultaneously or sequentially, which appears to be critical to guiding the pattern formation in real time. They demonstrate reversible transitions from flat to 1D ripple, to ripple with bifurcation, to ripple/herringbone mixed features, and to

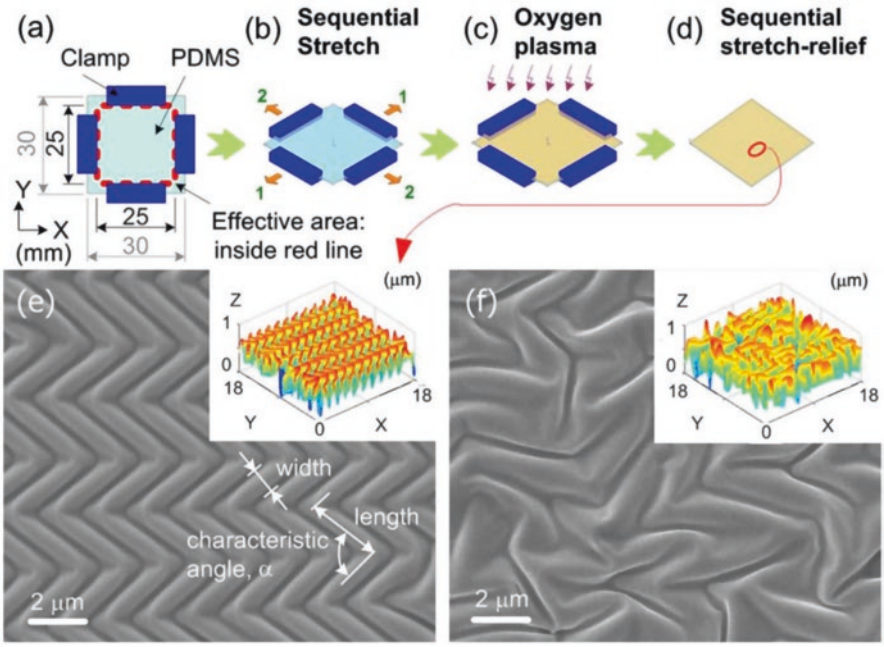

Fig. 2.12 Color online Schematic fabrication process to generate wrinkle patterns (**a**–**d**). SEM and AFM images of surface patterns when stretching/release of PDMS film either sequentially (**e**) or simultaneously (**f**). (Reproduced with permission from ref. [65])

the well-controlled formation of a highly ordered zigzag-based 2D herringbone structures.

An alternative strategy to fabricate two-dimensionally buckled structures was reported by Choi et al. [66]. As illustrated in Fig. 2.13, the authors casting and curing prepolymers of polydimethylsiloxane (PDMS) against polished silicon wafers generated planar elastomeric substrates. Exposure to an ozone environment created by intense ultraviolet light for 5 min converted the hydrophobic PDMS surface to a hydrophilic state. Heating such an activated PDMS substrate at 70–180 °C induced anisotropic thermal expansion. Contacting this heated film with silicon-on-insulator (SOI) wafers followed by a peeling permitted to transfer the entire nanomembrane to the PDMS. Finally, the nanomembrane/PDMS structure was cooled to room tem-

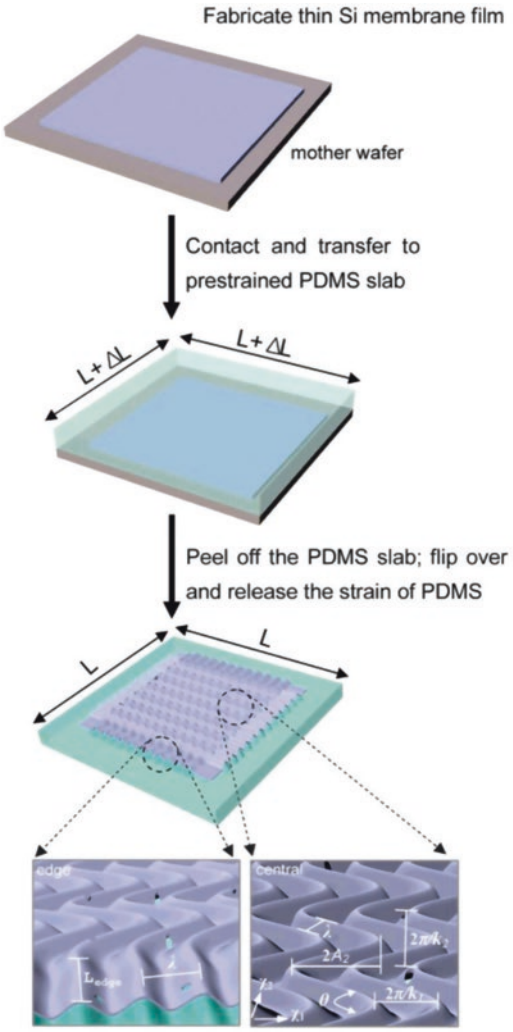

Fig. 2.13 Schematic illustration of steps for fabricating two-dimensional, "wavy" semiconductor nanomembranes on elastomeric supports. (Reproduced with permission from ref. [66])

perature (ca. 25 °C) to release the thermally induced pre-strain, thus leading to the spontaneous formation of two-dimensional (2D) wavy structures.

(c) *Swelling-induced wrinkles.*

Finally, wrinkle patterns can be also achieved by swelling usually induced by using a monomer solution but also solvents [23, 41, 67–75]. Upon immersion of the layered film using either a solvent vapor or a monomer mixture, regular wrinkles are formed. In this case, the final wrinkle characteristics, as well as the morphology, can be precisely controlled taking into account the solvent diffusion kinetics as well as the film characteristics including the geometry of the diffusion front or the cross-linking density [41].

For instance, Chan and Crosby [68] report an study in which a monomer diffusion is a basis to create microlens arrays and a variety of confined wrinkles. As depicted in Fig. 2.14, the authors employed a selective surface treatment (i.e., ultraviolet/ozone (UVO/O_3) oxidation) of polydimethylsiloxane (PDMS) to obtain a stiff silica thin film on top of the PDMS. As a result of this surface treatment, the required elastic-moduli differences on the PDMS surface are obtained and allowed the authors to control and define the wrinkle formation. In this case, a monomer was employed to induce the surface swelling. The authors coated the surface with photopolymerizable n-butyl acrylate (nBA) and then covered the system with a glass superstrate. Whereas the acrylate monomer swelled entirely the PDMS, the surface wrinkles were only observed in the oxidized PDMS regions where the moduli mismatch existed. As a result, this surface modification permits the control over the spatial distribution of the wrinkle patterns. Interestingly, the wrinkle morphology

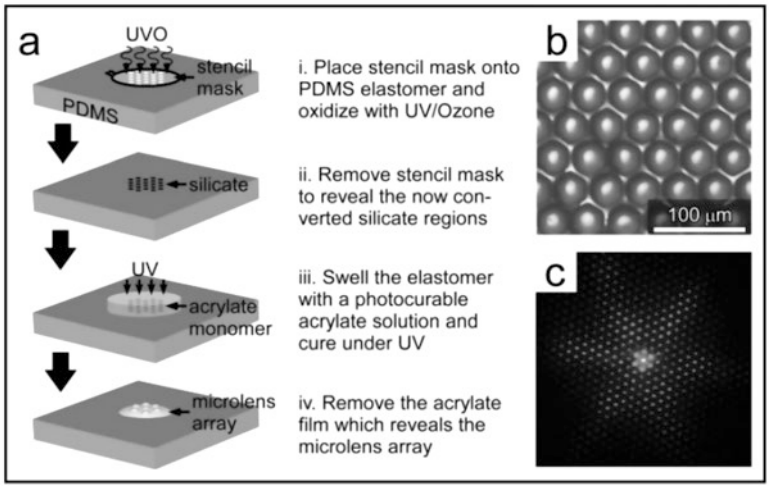

Fig. 2.14 (**a**) General scheme for fabricating the microlens arrays on a planar PDMS surface based on Chan and Crosby surface-wrinkling approach. (**b**) Optical microscopy image of the microlens array fabricated using our wrinkling process. (**c**) The diffraction pattern of the microlens illustrating uniformity of the array structure. (Reproduced with permission from ref. [68])

disappeared upon monomer evaporation but could be stabilized by photopolymerization of the nBA. Finally, we lifted away from the glass superstrate, which caused cohesive fracture of the polymerized poly(n-butyl acrylate) (PnBA) film and revealed the formation of the microlens (Fig. 2.14b).

As has been mentioned, the buckling process for microlens formation occurred as a result of the swelling of the moduli-mismatch oxidized PDMS regions. In a later contribution, [15] the authors demonstrated that the compressive stress can be finely tuned by changing the oxidation time and specific shape of the oxidized region. As a consequence, the control over the compressive stress state permitted both the creation of several forms of buckling structures and alignment of these wrinkle structures on both planar and nonplanar surfaces. Finally, the same authors [76] confirmed the capacity to fabricate reversible channels and microlens arrays by varying the area with local moduli mismatch as a function of the osmotic pressure (Fig. 2.15).

Another interesting example was reported by Vadeparre et al. [41, 73]. The authors described the preparation of bilayers following a two-step methodology. First, atactic polystyrene (PS) solutions in toluene were spin coated on bare silicon substrates to produce films with thicknesses around 0.25 μm. Then, a 15-nm-thick titanium (Ti) layer was placed onto the polymer surface by thermal evaporation. Using this hybrid bilayer configuration, wrinkling was induced by immersing the

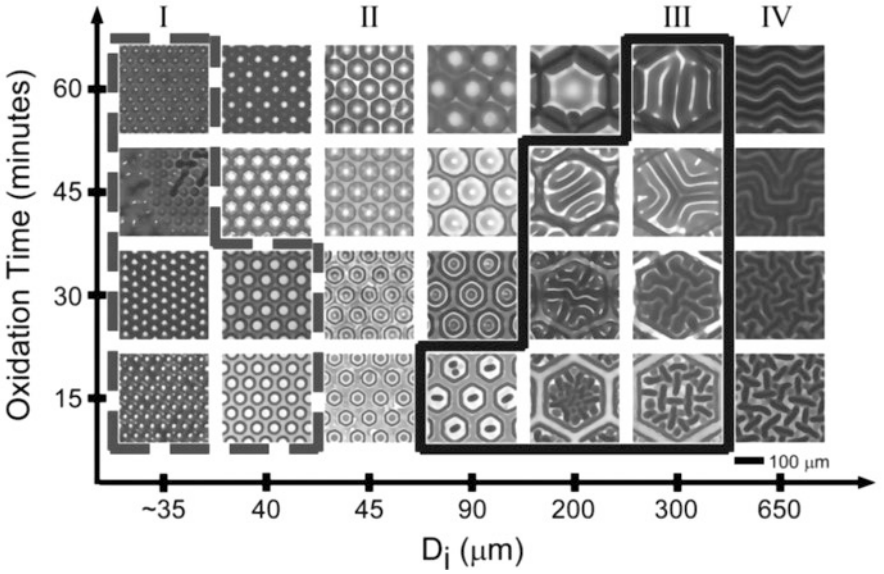

Fig. 2.15 (**a**) Morphologies of the wrinkled structures observed varying simultaneously the oxidation time and size of the oxidized region. For a nearly semi-infinite case, the random 2D wrinkled patterns were formed (IV). At low levels of confinement, we again observed the formation of 2D isotropic wrinkles (III). However, as we further decreased Di, lateral confinement played a significant role as the dimpled (II) and microlens (I) buckled structures were observed. (Reproduced with permission from ref. [68])

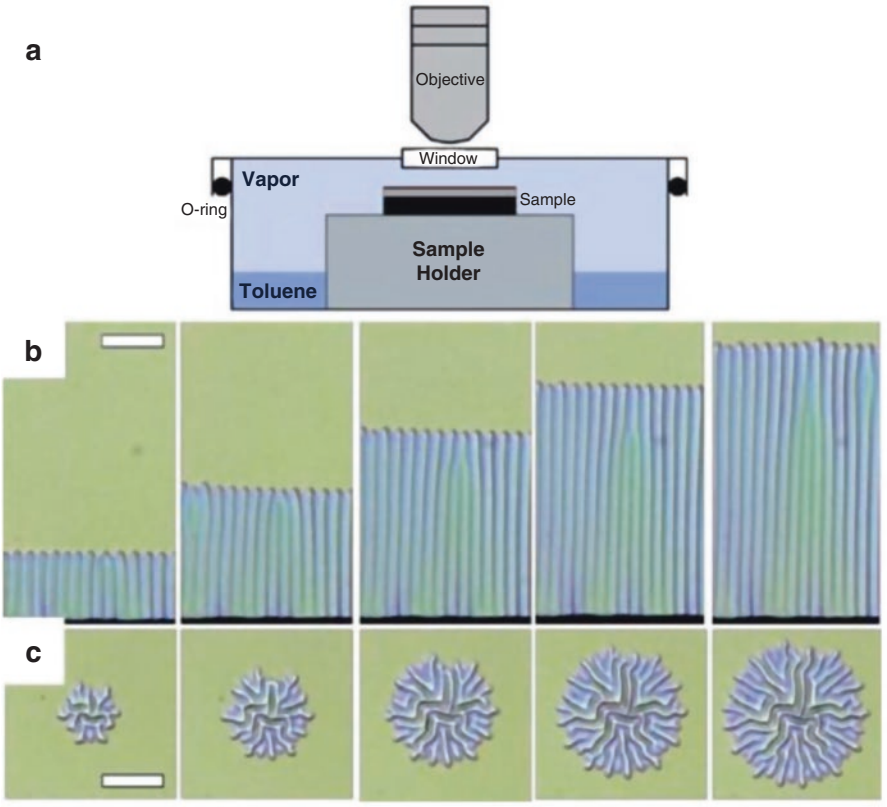

Fig. 2.16 (**a**) A schematic representation of the experimental setup. From left to right: Successive optical micrographs of (**b**) the growth of parallel and (**c**) radial wrinkled domains obtained after immersion of a Ti/PS/SiO_x trilayer in toluene vapors. The scale bar corresponds to 20 mm. (Reproduced with permission from ref. [41])

films in toluene vapor at room temperature since toluene is a good solvent for PS that can swell the polymer layer by diffusion through the Ti membrane. The wrinkle formation was followed by optical microscopy (Fig. 2.16), and the authors evidenced the formation of the hierarchical structure of folds. Interestingly, due to the diffusion process, this pattern shifts advancing as it grows, closely following the wave front.

2.4 Depth-Wise Gradient Films

As an alternative to the use of bilayered films described in the previous section, wrinkle formation on films with modulus gradient has been proven to form a wide range of surface microstructures ranging from peanuts, lamellar, and wormlike

shapes, among others, as well as to control of the film structure over large areas [77, 78]. Gradual cross-linked films fabricated as precursors for wrinkle formation have been prepared using several diverse alternatives including photo and thermal polymerization [79–81], cross-linked via polymer infusion [82], or selective polymerization of the film surface. [79, 83–85].

Basu et al. [79] are at the origin of the generally accepted mechanism of wrinkle formation in these systems. They established a comprehensive theory of wrinkle formation in curing coating systems validated for different curing conditions (thermal and UV), for a wide range of chemistry and independently of the delivery (liquid and powder). Wrinkle formation in gradient cross-linked films is depicted in Fig. 2.17 according to the theory developed by Basu et al. In this mechanism, a uniform thick film is cured either thermally or by UV irradiation or both. The initially liquid coating develops a gradient in degree of cross-linking and therefore in their mechanical properties. The top layer cross-linked to a larger extent and behaves like a solid skin. Upon further cross-linking of the film, the stress produced by the bulk developed and stabilized the wrinkle formation [7].

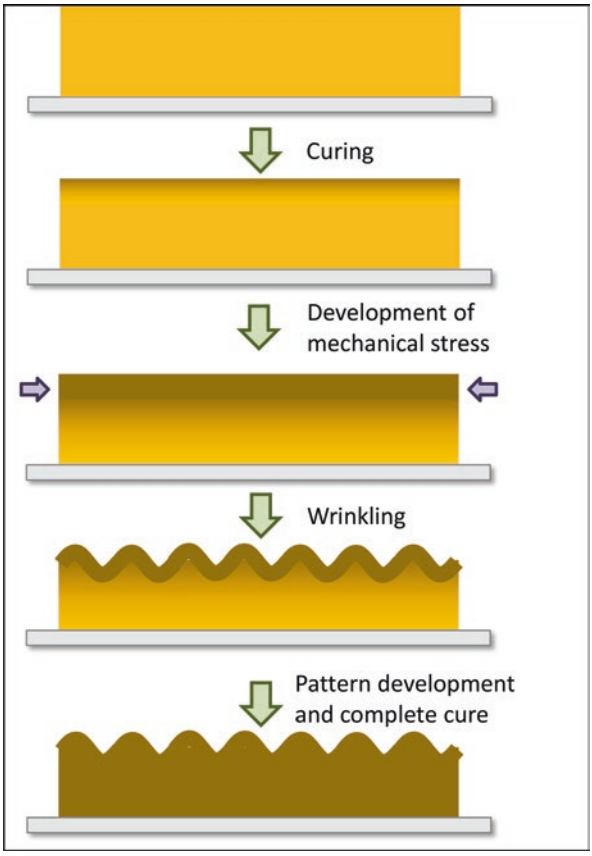

Fig. 2.17 Mechanism of wrinkle formation by gradient cross-linking polymerization. The cure occurs faster at the free surface, thus leading to the formation of a rigid layer. This layer will wrinkle as a consequence of the mechanical stress induced by the cross-linking of the bulk. (Figure adapted with permission from ref. [79])

As an alternative to the previously described one-step approach, other groups described recently strategies involving a two-step photocross-linking steps [86]. This approach, that requires two different irradiation steps, has been improved by Yang et al. [80] as well as Crosby et al. [81] that reduced the creation of wrinkled surface patterns to one-single step. In both strategies, a crucial aspect is the presence of oxygen diffusion in the top surface of the film which limits the polymerization in that particular region. Yang et al. [77] described the preparation of poly(hydroxyethyl methacrylate) (PHEMA) film from a partially polymerized HEMA embedded in a UV curable solution. For films with thicknesses above 20 μm, the amount of oxygen diffused into the film is gradually reduced, thus forming a film with gradually increasing cross-linked density (Fig. 2.18). In addition, initiator and cross-linker concentration, precursor viscosity or exposure time, and intensity will allow the fine-tuning of the gradient formed. As a result, upon swelling, distinctive patterns were observed including random, lamellar, peanut, or hexagonal.

A similar principle was employed by Crosby et al. [81]. They prepared a mixture of monomers and cross-linkers. Then the samples were irradiated with UV light, while a controlled oxygen flow was applied on the top of the sample. Similar to the example described above, at the monomer/air interface, a thin layer is formed where the radicals are quenched by the oxygen and the monomers remained uncured. Below a certain depth, the radical generation is higher than the oxygen inhibition, and cross-linking occurs. As a consequence, a cross-linking gradient is observed, thus leading to the generation of perpendicular stresses that finally provoke the formation of the surface wrinkles.

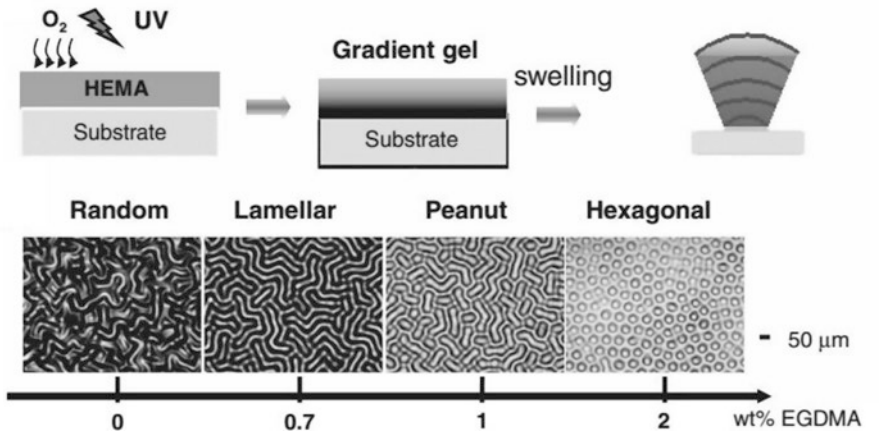

Fig. 2.18 Above: Schematic illustration of the fabrication of PHEMA films with a modulus gradient and formation of wrinkling patterns upon swelling. Below: Optical images of patterns on the surfaces of water-swollen PHEMA films. The order of the patterns is determined by the concentration of cross-linker EGDMA [77]. (Figure reproduced from ref. [80])

2.5 Homogeneous Films

Homogeneous films include films formed by using an elastoplastic polymer or homogeneously cross-linked gels. A large number of studies have been reported since the pioneer systematic study on the pattern formation in homogeneously polymerized gels carried out by Tanaka group [87, 88]. Inspired by these studies, a large variety of both experimental and theoretical studies have been equally reported [89–92]. Here below we will attempt to describe the different alternatives reported to fabricate surface wrinkles as a function of the stimulus employed.

2.5.1 Wrinkle Formation by Solvent Swelling/Drying

Swelling a polymeric thin film with a preferred solvent or monomer solution [68, 70, 72, 77, 78, 81, 93] is also an extended strategy to produce surface wrinkles inhomogeneous films. In a typical situation, the swelling-induced surface patterns are originated as a result of the selective swelling of the top of the film since the bottom of the polymer films is constrained as a consequence of the rigid interface [88]. This gradual swelling from the top to the bottom generates an anisotropic osmotic pressure along the film thickness that leads to a compressive strain of the film (Fig. 2.19). In the case that the compressive strain overcomes a critical value, the film surface start to buckle and finally produce surface wrinkles. While different authors [87, 88] employed swelling as a stimulus to produce surface wrinkles, this strategy entails two major limitations. One of the major problems is the difficulty to prepare wrinkles since other morphologies such as folds or creases are rapidly formed when large strains are achieved. The second issue is related to the nonlinearity of the swelling process that makes it difficult to obtain large-ordered wrinkled surfaces.

In addition to swelling, hydrogel shrinking can also induce mechanical instabilities [94, 95]. Pioneer studies on the patterns generated upon shrinking were carried

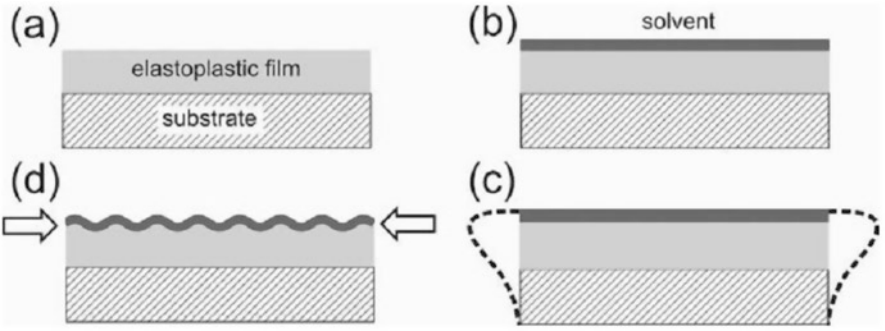

Fig. 2.19 Wrinkling formation by controlled solvent swelling (**a**) of a viscoelastic (elastoplastic) polymer film onto a rigid substrate. Upon swelling (**b**), the free top layer is selectively expanded (**c**) leading to a compressive strain and therefore to buckling (**d**). (Reproduced with permission from reference [80])

out by Matsuo and Tanaka [96]. Their preliminary works attempt to establish the mechanism involved in the generation of surface patterns and also to classify the different patterns generated in the form of a diagram. Figure 2.20 represents the phase diagram including all the patterns observed as a function of the combination of acetone and the final hydrogel length. As can be observed, volume phase transition in the hydrogels provokes also mechanical instabilities through deswelling that finally produced different patterns including bamboo, bubbles, or tubes.

Mechanical instability induced by drying, instead of the swelling, has also been exploited for the formation of wrinkled morphologies. However, in comparison to swelling, there are only a few reports on wrinkling of gels induced by drying. One of these studies was reported by Pauchard et al. [97, 98] who reported the wrinkle formation upon film drying. In particular, they studied experimentally the situations under which drop surface buckling occurs and their dependence on the drying rate and contact angle. They used concentrated solutions of the hydrosoluble polysaccharide dextran and demonstrated that the large shape distortions that occur during the drying of sessile drops of polymer solution are shown to be related to a buckling instability. As the solvent evaporates, polymers accumulate near the vapor/drop interface and, depending on the experimental conditions, can form a glassy skin which bends as the volume it encloses decreases.

In addition to the effect on drying films, Rizzieri et al. [99] explored the formation of wrinkles in stretched drying gelatin films (Fig. 2.21). When a thin film of initially hydrated gelatin is allowed to dry from the surface, superficial changes in the structure of the material affect the local mechanical properties of the drying region. If the film is simultaneously subjected to large strain deformation (above 20%), a periodic pattern of wrinkles appears on the surface of the gelatin along with the length of the sample in the direction of the applied force. These wrinkles were uniformly distributed on the surface of the gelatin with a wavelength that is much smaller than the sample thickness, which changes with sample composition, aging time, and deformation rate.

More recently, Huraux et al. [94] described the wrinkling of poly(vinyl alcohol) gels (PVA gels) induced by drying. Drying of PVA gel cylinders is performed under controlled humidity and ventilation (Figs. 2.22 and 2.23). The gels are dried in a drying chamber under a flow and controlled humidity (16–90%) and a precise temperature. Huraux et al. show that the drying-induced morphology of the gel is due to the crossing of the glass transition while varying the solvent concentration. They demonstrated that drying can induce wrinkling by forming a glassy skin layer which is compressed by the shrinkage of the core/bulk.

2.5.2 Wrinkles Produced Directly by Solvent Casting.

In contrast to cross-linked systems, a recent approach has been reported in which the formation of wrinkles occurs upon solvent casting of a polymer on a substrate without applying external stress. Ramanathan et al. [3] employed an

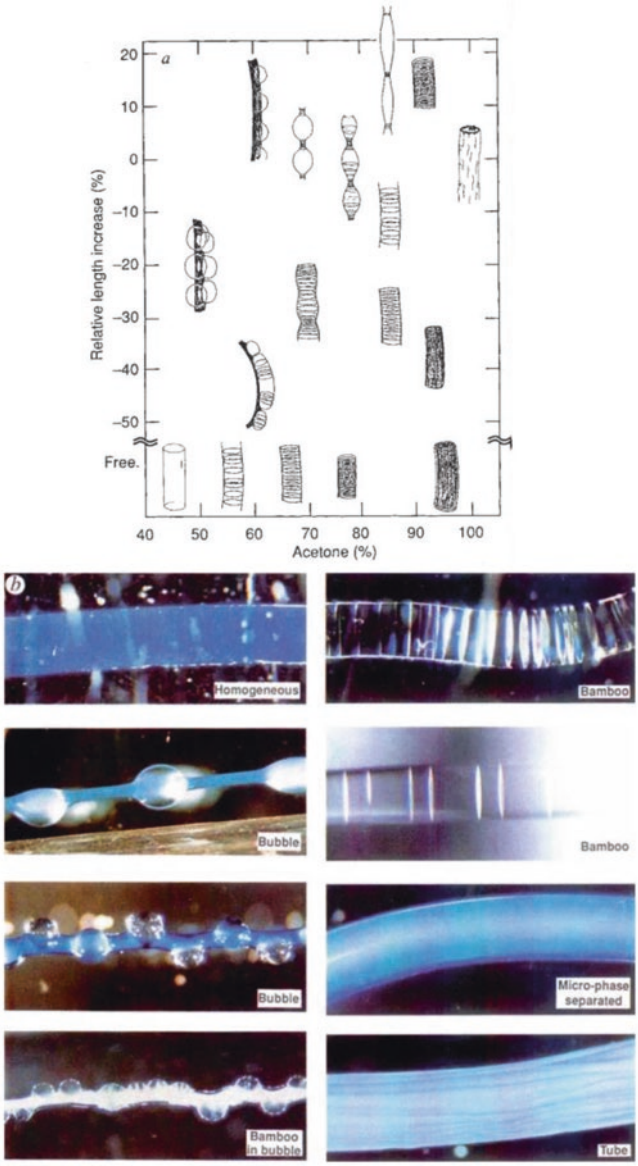

Fig. 2.20 (**a**) "Phase diagram" showing the regions of acetone concentration and fixed final length of a gel at which different patterns of cylindrical acrylamide hydrogels are formed. A negative relative length increase indicates that the fixed length was shorter than the original relaxed length, whereas a positive value means that the gel was stretched before shrinking. (**b**) Photographs that best represent the various patterns; some are ionic gels. (Reproduced with permission from ref. [96])

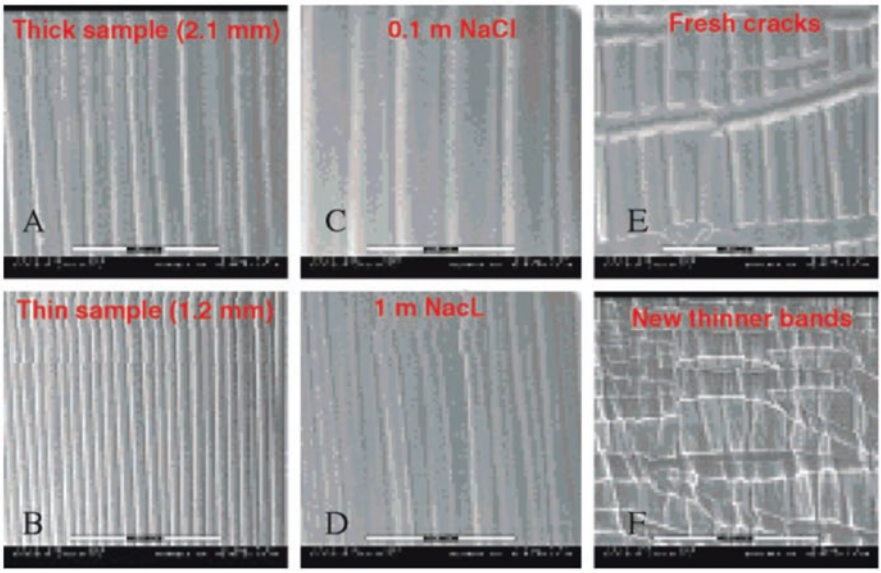

Fig. 2.21 Variation of the wrinkling wavelength, with the sample thickness [(**a**) 2.1 mm and (**b**) 1.2 mm], with the amount of NaCl [(**c**) 0.1 M and (**d**) 1 M], and on the new thinner bands at the opening of the horizontal cracks (E,F). (Reproduced with permission from ref. [99])

azalactone-based functional polymer and demonstrated that wrinkles are formed in a particular direction depending on the mode of deposition (Fig. 2.24). Moreover, given the spontaneity and versatility of wrinkle formation, they extended the use of this strategy to nonplanar geometries including tubes, cones, and other 3D structures. Equally, the authors used this approach to guide the deposition of metal nanoparticles and quantum dots, creating a periodic, nanopatterned film.

2.5.3 Wrinkles Produced by Marangoni Convection

Ellison and coworkers [100, 101] and Kim et al. [102] investigated the use of the Marangoni effect to produce the fluid flow in response to gradients in surface energy and produce nanoscale surface patterns.

On the one hand, Ellison and coworkers took advantage of the fact that exposure of polystyrene (PS) to ultraviolet (UV) light undertakes partial dehydrogenation of the alkane polymer backbone which increases its surface energy (Fig. 2.25). Based on this idea, the authors exposed polystyrene films to UV light using a photomask to induce a patterned photochemical reaction producing regions in the film with differing surface energy. Upon heating the solid polymer film with the preprogrammed surface energy pattern to a liquid state, the polymer flows from the low surface energy unexposed regions to high surface energy exposed regions. This flow creates

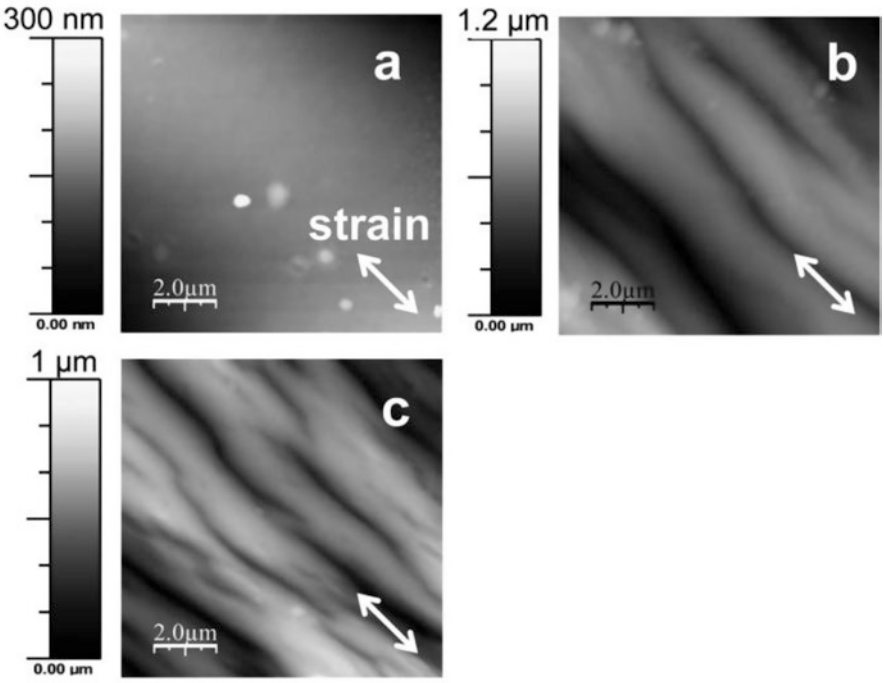

Fig. 2.22 Surface morphology of PVA gels dried at a fixed length under different humidities ((**a**) 85%, (**b**) 45%, (**c**) 12%) measured by AFM

three-dimensional topography by the Marangoni effect, which describes convective mass transfer due to surface energy gradients. The topographical features can be permanently preserved by quenching the film below its glass to the liquid transition temperature. Their shape and organization are only limited by the pattern on the photomask. In particular, thermal annealing above the glass transition temperature induces the flow of polymer from unexposed to exposed regions. As a result, a sinusoidal film thickness variations of 120 nm using a 12.5 µm half-pitch line and space mask.

The same group more recently [102] used the same Marangoni convection principle to generate microscale and nanoscale surface patterns using photosensitizers. In particular, the authors employed a near UV–visible light (NUV–vis) photosensitizer, 9,10-dibromo-anthracene (DBA) introduced into the thin films of poly(isobutyl methacrylate). As depicted in Fig. 2.26, upon light exposure through a photomask and heating above the glass transition, a flow of the film material into the exposed regions is observed.

Kim et al. [101] investigated the use of the Marangoni effect to produce the fluid flow in response to gradients in surface energy and produce nanoscale surface patterns. The procedure employed is depicted in Figs. 2.27 and 2.28. First, a poly(isobutyl methacrylate) (PiBMA) film containing 5 wt % 9,10-dibromo-

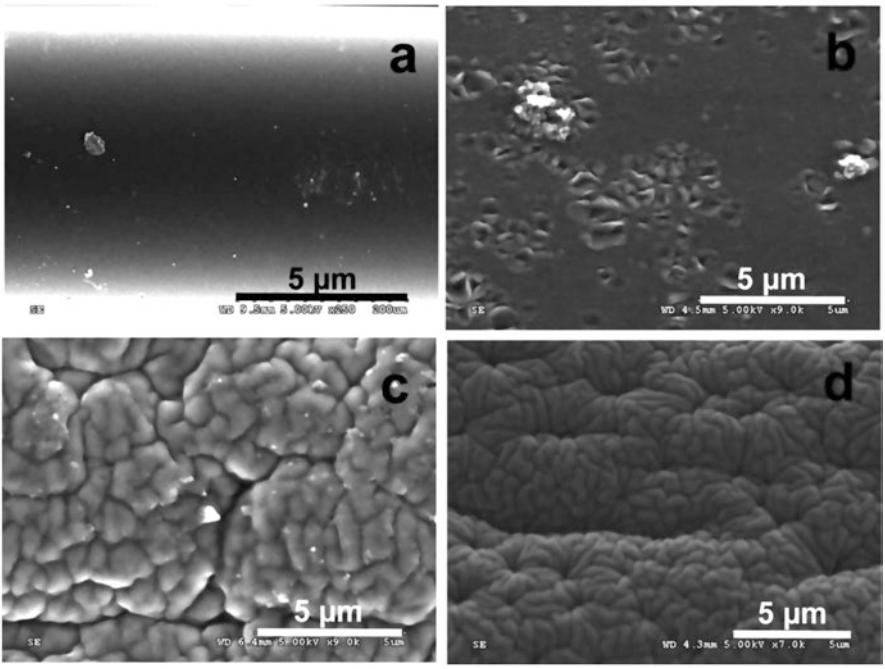

Fig. 2.23 Surface morphology of PVA gels dried with a free extremity under different values of humidity ((**a**) 95%, (**b**) 66%, (**c**) 47%, and (**d**) 16%) observed by SEM

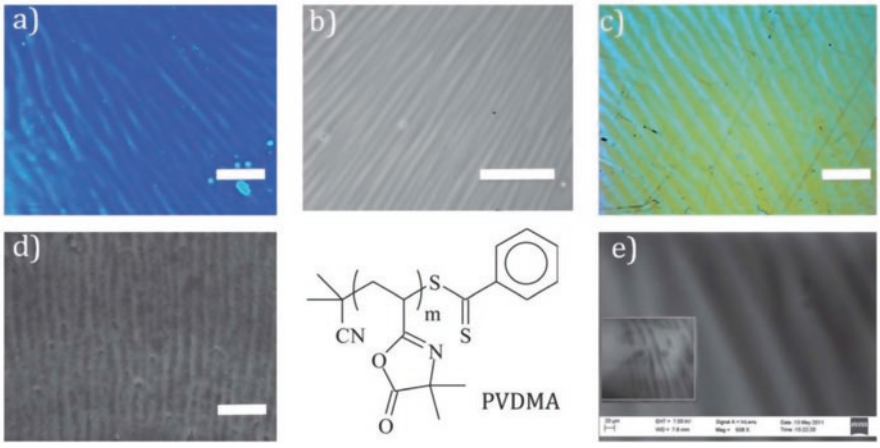

Fig. 2.24 Optical micrographs of wrinkling patterns that are formed by spin casting a 1 wt% solution of PVDMA in $CHCl_3$. (**a**), (**b**), and (**c**) represent the PVDMA wrinkles (in reflectance mode) on a variety of substrates such as nitride (Si3N4), oxide (SiOx), and noble metal (Au), respectively. (**d**) and (**e**) are a transmission optical micrograph (TOM) and a scanning electron micrograph (SEM) of PVDMA wrinkles, respectively. (Reproduced with permission from ref. [3])

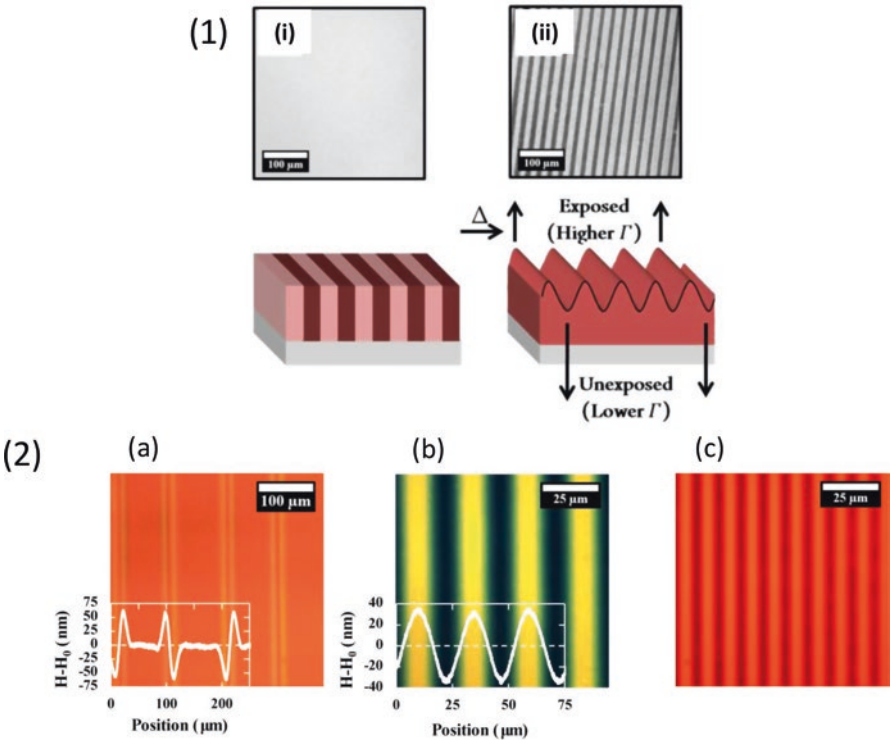

Fig. 2.25 (1) Schematic illustration of the steps involved in feature formation in a PS thin film. (i) A bright-field micrograph of a glassy polymer film (~150-nm-thick) after exposure to light through a photomask. No topography can be detected by atomic force microscopy after this stage. (ii) After heating the same film to 110 °C, where the polymer becomes a liquid, the patterned surface energy drives formation of topographic features via the Marangoni effect. (2) Patterns created in ~150-nm-thick PS films with overlaid profilometry traces showing topography formed by using photomasks with different line spacing of (**a**) 100 μm chrome lines with a 200 μm pitch, (**b**) 12.5 μm chrome lines on a 25 μm pitch, and (**c**) 5 μm chrome lines on a 10 μm pitch. (Reproduced with permission from refs. [100, 101])

anthracene (DBA) was spin coated onto a silicon wafer. Then, a NUV–vis light exposure was applied through a photomask, and the DBA was photochemically oxidized in the exposed regions. Finally, upon thermal annealing above the T_g and due to the Marangoni effect, polymer flows into the exposed regions from the unexposed regions. This results in a film with a smoothly varying thickness profile reflective of the photomask pattern.

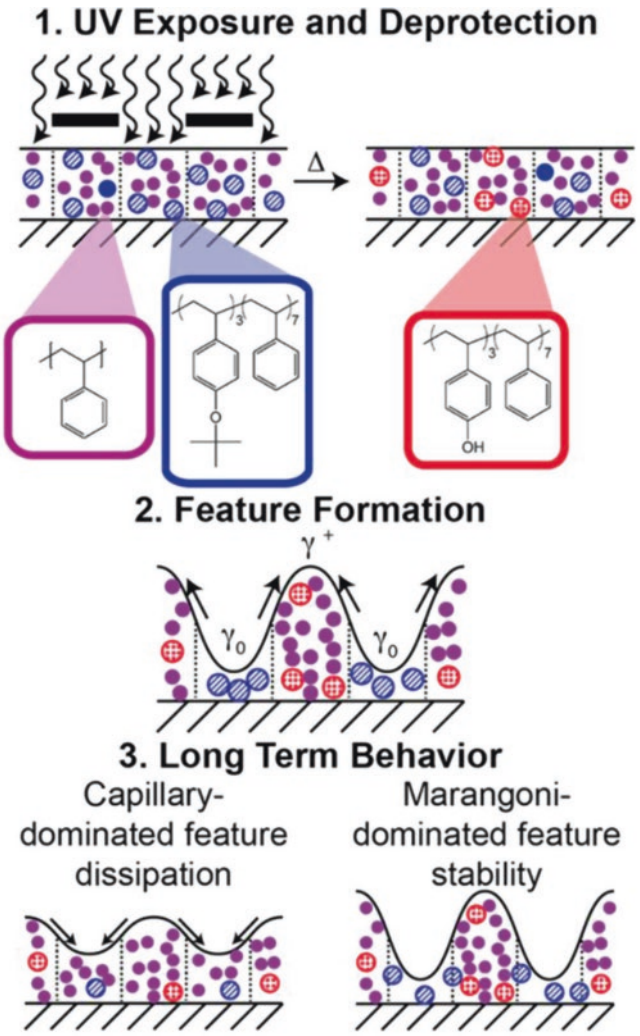

Fig. 2.26 Polymer patterning methodology. (1) Schematic of the polymer blend which is composed of a low molecular weight PS (solid purple) and a high molecular weight copolymer, P(tBOS-ran-S) (blue hashed circles). Spatial control of the surface energy gradient is achieved by exposing films through a photomask, and the subsequent annealing of these films leads to a photochemical transformation of P(tBOS-ran-S) into P(HOST-ran-S) (red dotted circles) with the aid of a photoacid generator. (2) With extended annealing time, polymer flows from regions of low to high surface energy, and (3) the long-term behavior (dissipation or stability of topography) is determined by whether capillary or Marangoni forces dominate, respectively. (Reproduced with permission from ref. [102])

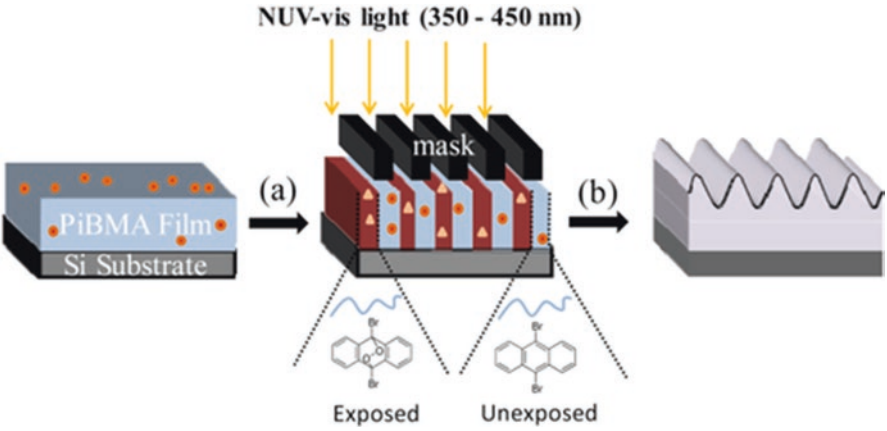

Fig. 2.27 Patterning schematic of (**a**) NUV–vis light exposure in an ambient air atmosphere and (**b**) subsequent thermal annealing. Exposed regions (higher surface energy) rise, while the unexposed regions (lower surface energy) sink upon thermal annealing. (Reproduced with permission from ref. [101])

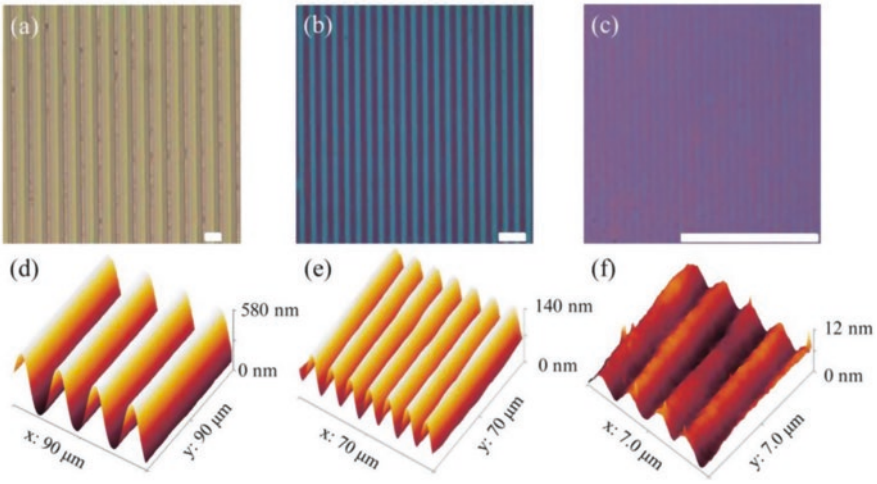

Fig. 2.28 Optical micrographs of the patterned samples using (**a**) 12.5 μm, (**b**) 5 μm, and (**c**) 800 nm half-pitch "line and space" masks. All scale bars indicate 25 μm. AFM images of the corresponding patterned samples are shown below. Initial film thicknesses were 300 nm. All samples were exposed to light for 15 min. (Reproduced with permission from ref. [101])

2.5.4 Film Wrinkling under Capillary Forces

Examples of wrinkling of films under capillary forces are rather rare in spite that very often thin films are dipped in fluid environments. As a result, thin films are usually exposed to different deformations and surface tensions. An illustrative example of wrinkling under capillary forces was reported by Huang et al. [8]. They studied films based on high molecular weight polystyrene with a high aspect ratio (the ratio of the

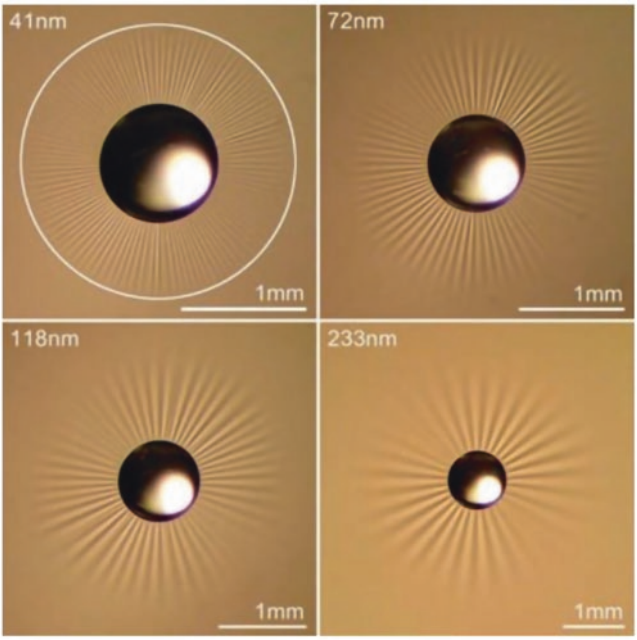

Fig. 2.29 Four PS films of diameter D = 22.8 mm and of varying thicknesses floating on the surface of water, each wrinkled by water drops of radius a ≈ 0.5 mm and mass m ≈ 0.2 mg. As the film is made thicker, the number of wrinkles N decreases (there are 111, 68, 49, and 31 wrinkles in these images), and the length of wrinkles L increases. (Reproduced with permission from ref. [8])

diameter D to thickness h is $D/h \sim 5 \times 10^5$) spin coated onto glass substrates (Fig. 2.29). The film thickness h was varied from 31 to 233 nm. Because PS is hydrophobic, the film floated to the surface of the water where it was stretched flat by the surface tension of the air-water interface at its perimeter. Wrinkles were induced in the stretched, floating film by placing a drop of water in the center of the film by placing a solid disk in the center of the film. Later, Vella et al. [9] described a physically based model for the deformation of a floating elastic membrane caused by the presence of a liquid drop that explains the wrinkle formation observed by Huang et al. [8]. The authors started using the equations of membrane theory modified to account for surface energies to evidence that the presence of a liquid drop causes an azimuthal compression over a finite region determining the extent of the wrinkled region.

2.5.5 Direct Laser Interference Patterning (DLIP)

Direct laser interference patterning (DLIP) permits through the selective surface ablation the design of a wide range of surface patterns in polymers in a single-step process. In particular, DLIP is an alternative methodology for the direct fabrication of periodic arrays [103]. As depicted in Fig. 2.30, this method involves the irradiation of the sample surface with two or more coherent laser beams, thus producing a

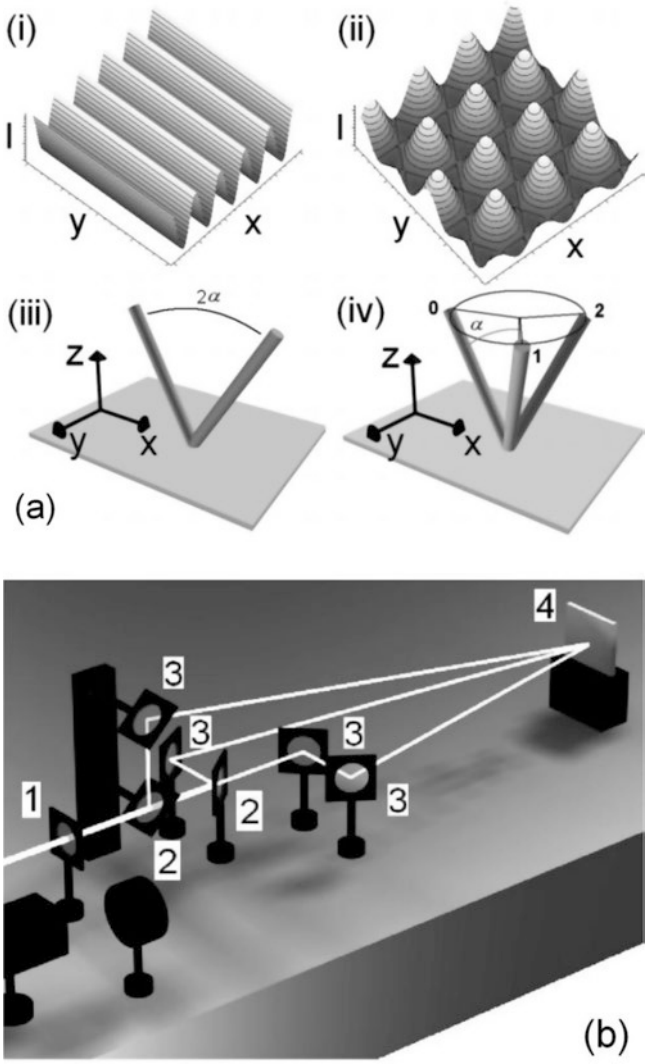

Fig. 2.30 (**a**) Two- and three-laser beam interference patterns: (i) Line-type pattern with corresponding two-laser beam (iii) configuration; (ii) dot-type pattern with corresponding three-laser beam; (iii) symmetrical configuration. (**b**) Experimental setup for three-laser beam interference experiments: (1) Lens; (2) mirror; (3) beam splitter; (4) sample. (Reproduced with permission from ref. [105])

periodic distribution of laser intensity due to the phenomenon of interference [104]. This methodology requires the use of high-power lasers, and by the interaction of these lasers with the surface of different materials, these can be directly modified leading to periodic arrays with features in the micro-/nanoscale on macroscopic areas [105]. In comparison to other alternative lithographic methods, DLIP has a distinctive advantage since no additional process steps are required (i.e., etching, development of photoresist) [106].

As will be thoroughly described in Chap. 7, a wide variety of polymeric materials can be microstructured using this methodology. For instance, polymer typically employed for the fabrication of different biomedical devices such as poly(etherimide) (PEI) is used in harmonic scalpels, poly(imide) (PI) is used in off-pump coronary artery bypass devices, polycarbonate (PC) is used in electrophysiology catheters or poly(ether ether ketone) (PEEK) resists sterilization by radiation or heat treatment, and it has been used to produce kidney dialysis machine components [105]. This methodology permits also the surface microstructuration of conductive polymers that usually present limited solubility such as PANI [107, 108] or fabricate linear structures in PEDOT-PSS films with ns-lasers [109] and also form complex surface patterns using copolymers such as polystyrene-polymethyl methacrylate copolymers [110].

2.5.6 Laser-Induced Periodic Surface Structures (LIPPS)

In addition to DLIP, an alternative approach has been reported in which the polymer surface is illuminated by using a pulsed laser source with gentle fluences. This pulsed irradiation allows for the formation of different period structures, and the methodology is known as laser-induced periodic surface structures (LIPSS) [111–114]. An abundant diversity of experimental work has been reported during the last years on LIPSS, and as a result, different theoretical approaches have been developed [115, 116]. In spite of the large number of works devoted to the use of LIPSS, only a few of them focus on the structuration of polymers with femtosecond lasers.

Pioneer experiments carried out by Baudach et al. [117] reported the formation of microstructures by ablation on polyimide (PI) with femtosecond laser pulses. The same group extended this work to other polymeric materials such as polycarbonate (PC), polyethylene terephthalate (PET), polytetrafluoroethylene (PTFE), and polymethylmethacrylate (PMMA) [118]. In these preliminary works assumed, the authors assumed that ablation was at the origin of the microstructuration. However, as mentioned by Forster et al. [119], ablation can potentially alter not only the chemical but also the physical properties of the polymer. These can include the altered optical absorption and, in particular, for PI, increased electrical conductivity due to carbonization of the surface.

In order to avoid ablation, Forster et al. [119] applied ultrashort laser pulses tailored on a picosecond time scale to study the influence of different pulse durations (150 fs–5 ps) and double pulses (with time delays between 300 fs and 11 ps) on the formation of ripples on PI, taking into account the nonlinearity of interaction but also the dynamics of phase transitions. Interestingly, according to their findings, the process of ripple formation is correlated to material properties as, e.g., the electron-phonon relaxation time. In this case, the amount of material removed from the surface is negligible, so the formation of ripples is mainly due to a self-organization process.

By using the simplest configuration, LIPPS generally forms ripples at the surface, and the periodicity corresponds approximately to the wavelength of the laser radiation employed. The pattern formation has been attributed to the interference

between the incident and scattered light or excited surface waves [120]. More precisely, the interference between incident linearly polarized light and the surface-scattered wave generated during the pulse leads to a periodic modulation of the absorbed light intensity and, consequently to a modulated surface roughening which enhances the development of the structures [121].

As an illustrative example (see Chap. 6 for more information about this method), Rebollar et al. [121] employed three different polymers, i.e., poly(ethylene terephthalate) (PET), poly(trimethylene terephthalate) (PTT), and polycarbonate bisphenol A (PC), to study the laser parameters in order to form homogeneous patterned surfaces. Figure 2.31 shows illustrative AFM height images of PET, PTT, and PC irradiated at 265 nm with 5000 pulses at different fluences ranging from 1.1 to −1.6 mJ/cm^2. Whereas for low fluences (F < 1 mJ/cm^2), no morphological changes

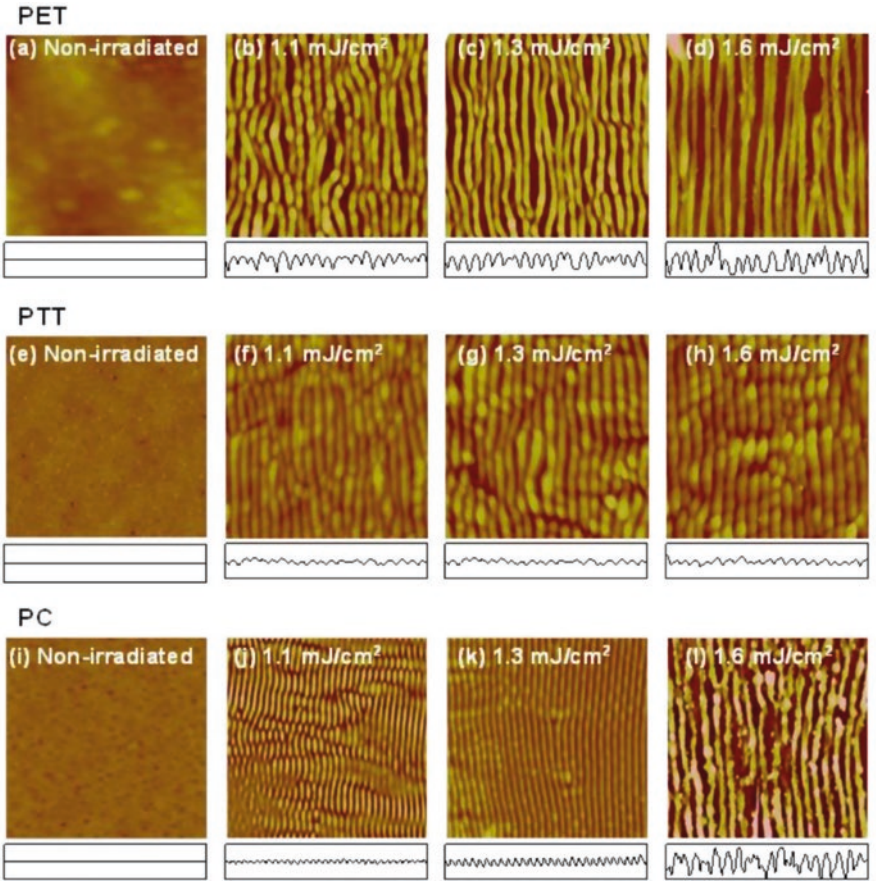

Fig. 2.31 AFM height images (5 × 5 μm^2) of PET, PTT, and PC irradiated at 265 nm with 5000 pulses at the indicated fluences. Images of as-spun polymers are shown as a reference. The height profile along a 5 μm line perpendicular to the ripples is shown below every image (height scale: 250 nm). (Reproduced with permission from ref. [121])

were observed at the polymer surface increasing the fluence above 1 mJ/cm^2, structures start to be formed and develop the form of parallel and well-defined ripples. Moreover, upon further increase of the fluence at approximately 1.6–1.9 mJ/cm^2, LIPSS start to distort indicating that an optimum range of irradiation intensity is required to obtain well-defined surface structures.

2.6 Conclusions

This chapter attempt to briefly describe, in an organized manner, the different alternatives reported producing micro- and nano-wrinkled surface structures. A wide variety of strategies have been reported that are classified as a function of the film structure, i.e., layered films, depth-wise gradient films, and homogeneous films.

Swelling, temperature, mechanical stretching, or even the irradiation with light or lasers are at the origin of the creation of surface instabilities that finally lead to the formation of wrinkles with variable sizes (from nano- to micrometer scale) and eventually particular orientations (random, parallel, or following the morphologies of pre-patterned substrates).

The large number of existing methodologies that finally offers alternatives to produce micropatterned substrates with controlled morphology as well as with variable chemical composition with potential for multiple applications as will be thoroughly described in Chaps. 12, 13, and 14.

Acknowledgments The authors acknowledge financial support given by FONDECYT grant N° 1170209. M.A. Sarabia acknowledges the financial support given by CONICYT through the doctoral program scholarship grant. J. Rodriguez-Hernandez acknowledges financial support from Ministerio de Economia y Competitividad (MINECO) (Project MAT2016-78437-R, FEDER EU). Finally, this study was funded by VRAC grant number L216-04 of Universidad Tecnológica Metropolitana.

References

1. P. Gruner, M. Arlt, T. Fuhrmann-Lieker, Surface wrinkling induced by photofluidization of low molecular azo glasses. ChemPhysChem **14**(2), 424–430 (2013)
2. N. Lambricht, T. Pardoen, S. Yunus, Giant stretchability of thin gold films on rough elastomeric substrates. Acta Mater. **61**(2), 540–547 (2013)
3. M. Ramanathan, B.S. Lokitz, J.M. Messman, C.M. Stafford, S.M. Kilbey II, Spontaneous wrinkling in azlactone-based functional polymer thin films in 2D and 3D geometries for guided nanopatterning. J. Mater. Chem. C **1**(11), 2097–2101 (2013)
4. Z. Wu, N. Bouklas, R. Huang, Swell-induced surface instability of hydrogel layers with material properties varying in thickness direction. Int. J. Solids Struct. **50**(3–4), 578–587 (2013)
5. Z. Chen, Y.Y. Kim, S. Krishnaswamy, Anisotropic wrinkle formation on shape memory polymer substrates. J. Appl. Phys. **112**(12) (2012)

6. Y.-C. Chen, A.J. Crosby, Wrinkling of inhomogeneously strained thin polymer films. Soft Matter **9**(1), 43–47 (2013)
7. J. Rodríguez-Hernández, Wrinkled interfaces: Taking advantage of surface instabilities to pattern polymer surfaces. Prog. Polym. Sci. **42**, 1–41 (2015)
8. J. Huang, M. Juszkiewicz, W.H. De Jeu, E. Cerda, T. Emrick, N. Menon, T.P. Russell, Capillary wrinkling of floating thin polymer films. Science **317**(5838), 650–653 (2007)
9. D. Vella, M. Adda-Bedia, E. Cerda, Capillary wrinkling of elastic membranes. Soft Matter **6**(22), 5778–5782 (2010)
10. D.P. Holmes, A.J. Crosby, Draping films: A wrinkle to fold transition. Phys. Rev. Lett. **105**(3), 038303 (2010)
11. L. Pocivavsek, R. Dellsy, A. Kern, S. Johnson, B. Lin, K.Y.C. Lee, E. Cerda, Stress and fold localization in thin elastic membranes. Science **320**(5878), 912–916 (2008)
12. N. Sridhar, D. Srolovitz, Z. Suo, Kinetics of buckling of a compressed film on a viscous substrate. Appl. Phys. Lett. **78**(17), 2482–2484 (2001)
13. R. Huang, Z. Suo, Wrinkling of a compressed elastic film on a viscous layer. J. Appl. Phys. **91**(3), 1135–1142 (2002)
14. S. Chatterjee, C. McDonald, J. Niu, S.S. Velankar, P. Wang, R. Huang, Wrinkling and folding of thin films by viscous stress. Soft Matter **11**(9), 1814–1827 (2015)
15. R. Huang, Kinetic wrinkling of an elastic film on a viscoelastic substrate. J. Mech. Phys. Solids **53**(1), 63–89 (2005)
16. S. Im, R. Huang, Evolution of wrinkles in elastic-viscoelastic bilayer thin films. J. Appl. Mech. **72**(6), 955–961 (2005)
17. R. Huang, S.H. Im, Dynamics of wrinkle growth and coarsening in stressed thin films. Phys. Rev. E **74**(2), 026214 (2006)
18. K. Dalnoki-Veress, J. Forrest, J. Dutcher, Mechanical confinement effects on the phase separation morphology of polymer blend thin films. Phys. Rev. E **57**(5), 5811 (1998)
19. P.J. Yoo, K.Y. Suh, S.Y. Park, H.H. Lee, Physical self-assembly of microstructures by anisotropic buckling. Adv. Mater. **14**(19), 1383–1387 (2002)
20. T. Okayasu, H.L. Zhang, D.G. Bucknall, G.A.D. Briggs, Spontaneous formation of ordered lateral patterns in polymer thin-film structures. Adv. Funct. Mater. **14**(11), 1081–1088 (2004)
21. P.J. Yoo, H.H. Lee, Morphological diagram for metal/polymer bilayer wrinkling: Influence of thermomechanical properties of polymer layer. Macromolecules **38**(7), 2820–2831 (2005)
22. E.P. Chan, K.A. Page, S.H. Im, D.L. Patton, R. Huang, C.M. Stafford, Viscoelastic properties of confined polymer films measured via thermal wrinkling. Soft Matter **5**(23), 4638–4641 (2009)
23. P.J. Yoo, H.H. Lee, Evolution of a stress-driven pattern in thin bilayer films: Spinodal wrinkling. Phys. Rev. Lett. **91**(15), 154502 (2003)
24. K. Srinivasan, G. Subbarayan, T. Siegmund, Wrinkling on irreversibly deforming foundations. Thin Solid Films **520**(17), 5671–5682 (2012)
25. A. El Haitami, F. Bretagnol, P. Assuid, G. Petitet, S. Cantournet, L. Corté, Erasable and reversible wrinkling of halogenated rubber surfaces. Langmuir **29**(50), 15664–15672 (2013)
26. N. Bowden, W.T.S. Huck, K.E. Paul, G.M. Whitesides, The controlled formation of ordered, sinusoidal structures by plasma oxidation of an elastomeric polymer. Appl. Phys. Lett. **75**(17), 2557–2559 (1999)
27. D.B.H. Chua, H.T. Ng, S.F.Y. Li, Spontaneous formation of complex and ordered structures on oxygen-plasma-treated elastomeric polydimethylsiloxane. Appl. Phys. Lett. **76**(6), 721–723 (2000)
28. C.-C. Fu, A. Grimes, M. Long, C.G.L. Ferri, B.D. Rich, S. Ghosh, S. Ghosh, L.P. Lee, A. Gopinathan, M. Khine, Tunable Nanowrinkles on shape memory polymer sheets. Adv. Mater. **21**(44), 4472 (2009)
29. X.M. Zhao, Y.N. Xia, O.J.A. Schueller, D. Qin, G.M. Whitesides, Fabrication of microstructures using shrinkable polystyrene films. Sens. Actuators A Phys. **65**(2–3), 209–217 (1998)

30. Y. Zhao, W.M. Huang, Y.Q. Fu, Formation of micro/nano-scale wrinkling patterns atop shape memory polymers. J. Micromech. Microeng. **21**(6) (2011)
31. M.D. Huntington, C.J. Engel, A.J. Hryn, T.W. Odom, Polymer Nanowrinkles with continuously tunable wavelengths. ACS Appl. Mater. Interfaces **5**(13), 6438–6442 (2013)
32. P. Kim, M. Abkarian, H.A. Stone, Hierarchical folding of elastic membranes under biaxial compressive stress. Nat. Mater. **10**(12), 952–957 (2011)
33. A. Verma, A. Sharma, G.U. Kulkarni, Ultrafast large-area micropattern generation in nonabsorbing polymer thin films by pulsed laser diffraction. Small **7**(6), 758–765 (2011)
34. M.-W. Moon, S.H. Lee, J.-Y. Sun, K.H. Oh, A. Vaziri, J.W. Hutchinson, Wrinkled hard skins on polymers created by focused ion beam. Proc. Natl. Acad. Sci. U. S. A. **104**(4), 1130–1133 (2007)
35. N. Bowden, S. Brittain, A.G. Evans, J.W. Hutchinson, G.M. Whitesides, Spontaneous formation of ordered structures in thin films of metals supported on an elastomeric polymer. Nature **393**(6681), 146–149 (1998)
36. W.T.S. Huck, N. Bowden, P. Onck, T. Pardoen, J.W. Hutchinson, G.M. Whitesides, Ordering of spontaneously formed buckles on planar surfaces. Langmuir **16**(7), 3497–3501 (2000)
37. P.J. Yoo, K.Y. Suh, H. Kang, H.H. Lee, Polymer elasticity-driven wrinkling and coarsening in high temperature buckling of metal-capped polymer thin films. Phys. Rev. Lett. **93**(3) (2004)
38. S.J. Kwon, P.J. Yoo, H.H. Lee, Wave interactions in buckling: Self-organization of a metal surface on a structured polymer layer. Appl. Phys. Lett. **84**(22), 4487–4489 (2004)
39. P.J. Yoo, S.Y. Park, S.J. Kwon, K.Y. Suh, H.H. Lee, Microshaping metal surfaces by wave-directed self-organization. Appl. Phys. Lett. **83**(21), 4444–4446 (2003)
40. P.J. Yoo, H.H. Lee, Evolution of a stress-driven pattern in thin bilayer films: Spinodal wrinkling. Phys. Rev. Lett. **91**(15) (2003)
41. H. Vandeparre, S. Gabriele, F. Brau, C. Gay, K.K. Parker, P. Damman, Hierarchical wrinkling patterns. Soft Matter **6**(22), 5751–5756 (2010)
42. C.M. Stafford, B.D. Vogt, C. Harrison, D. Julthongpiput, R. Huang, Elastic moduli of ultrathin amorphous polymer films. Macromolecules **39**(15), 5095–5099 (2006)
43. K.Y. Suh, S.M. Seo, P.J. Yoo, H.H. Lee, Formation of regular nanoscale undulations on a thin polymer film imprinted by a soft mold. J. Chem. Phys. **124**(2) (2006)
44. M. Watanabe, H. Shirai, T. Hirai, Wrinkled polypyrrole electrode for electroactive polymer actuators. J. Appl. Phys. **92**(8), 4631–4637 (2002)
45. J. Yang, S. Damle, S. Maiti, S.S. Velankar, Stretching-induced wrinkling in plastic–rubber composites. Soft Matter **13**(4), 776–787 (2017)
46. D. Rhee, W.K. Lee, T.W. Odom, Crack-free, soft wrinkles enable switchable anisotropic wetting. Angew. Chem. Int. Ed. **56**(23), 6523–6527 (2017)
47. T. Boudou, T. Crouzier, K. Ren, G. Blin, C. Picart, Multiple functionalities of polyelectrolyte multilayer films: New biomedical applications. Adv. Mater. **22**(4), 441–467 (2010)
48. Y. Wang, A.S. Angelatos, F. Caruso, Template synthesis of nanostructured materials via layer-by-layer assembly. Chem. Mater. **20**(3), 848–858 (2008)
49. Z. Tang, Y. Wang, P. Podsiadlo, N.A. Kotov, Biomedical applications of layer-by-layer assembly: From biomimetics to tissue engineering. Adv. Mater. **18**(24), 3203–3224 (2006)
50. P.T. Hammond, Form and function in multilayer assembly: New applications at the nanoscale. Adv. Mater. **16**(15), 1271–1293 (2004)
51. C. Lu, H. Mohwald, A. Fery, A lithography-free method for directed colloidal crystal assembly based on wrinkling. Soft Matter **3**(12), 1530–1536 (2007)
52. J. Kim, H.H. Lee, Wave formation by heating in thin metal film on an elastomer. J. Polym. Sci. B Polym. Phys. **39**(11), 1122–1128 (2001)
53. T. Okayasu, H.L. Zhang, D.G. Bucknal, G. Andrew, D. Briggs, Spontaneous formation of ordered lateral patterns in polymer thin-film structures. Adv. Funct. Mater. **14**(11), 1081–1088 (2004)
54. P.J. Yoo, Invited paper: Fabrication of complexly patterned wavy structures using self-organized anisotropic wrinkling. Electron. Mater. Lett. **7**(1), 17–23 (2011)

55. P.J. Yoo, H.H. Lee, Complex pattern formation by adhesion-controlled anisotropic wrinkling. Langmuir **24**(13), 6897–6902 (2008)
56. C. Jiang, S. Singamaneni, E. Merrick, V.V. Tsukruk, Complex buckling instability patterns of nanomembranes with encapsulated gold nanoparticle arrays. Nano Lett. **6**(10), 2254–2259 (2006)
57. T.R. Hendricks, I. Lee, Wrinkle-free nanomechanical film: Control and prevention of polymer film buckling. Nano Lett. **7**(2), 372–379 (2006)
58. D. Mertz, J. Hemmerlé, J. Mutterer, S. Ollivier, J.-C. Voegel, P. Schaaf, P. Lavalle, Mechanically responding Nanovalves based on polyelectrolyte multilayers. Nano Lett. **7**(3), 657–662 (2007)
59. C.M. Stafford, C. Harrison, K.L. Beers, A. Karim, E.J. Amis, M.R. Vanlandingham, H.C. Kim, W. Volksen, R.D. Miller, E.E. Simonyi, A buckling-based metrology for measuring the elastic moduli of polymeric thin films. Nat. Mater. **3**(8), 545–550 (2004)
60. A.J. Nolte, M.F. Rubner, R.E. Cohen, Determining the young's modulus of polyelectrolyte multilayer films via stress-induced mechanical buckling instabilities. Macromolecules **38**(13), 5367–5370 (2005)
61. R.C. Hedden, H. Saxena, C. Cohen, Mechanical properties and swelling behavior of end-linked poly(diethylsiloxane) networks. Macromolecules **33**(23), 8676–8684 (2000)
62. K. Efimenko, M. Rackaitis, E. Manias, A. Vaziri, L. Mahadevan, J. Genzer, Nested self-similar wrinkling patterns in skins. Nat. Mater. **4**(4), 293 (2005)
63. T. Ohzono, M. Shimomura, Ordering of microwrinkle patterns by compressive strain. Phys. Rev. B **69**(13), 132202 (2004)
64. T. Ohzono, M. Shimomura, Geometry-dependent stripe rearrangement processes induced by strain on preordered microwrinkle patterns. Langmuir **21**(16), 7230–7237 (2005)
65. P.-C. Lin, S. Yang, Spontaneous formation of one-dimensional ripples in transit to highly ordered two-dimensional herringbone structures through sequential and unequal biaxial mechanical stretching. Appl. Phys. Lett. **90**(24), 241903 (2007)
66. W.M. Choi, J. Song, D.-Y. Khang, H. Jiang, Y.Y. Huang, J.A. Rogers, Biaxially stretchable "wavy" silicon nanomembranes. Nano Lett. **7**(6), 1655–1663 (2007)
67. H.S. Kim, A.J. Crosby, Solvent-responsive surface via wrinkling instability. Adv. Mater. **23**(36), 4188 (2011)
68. E.P. Chan, A.J. Crosby, Fabricating microlens arrays by surface wrinkling. Adv. Mater. **18**(24), 3238–3242 (2006)
69. J.Y. Chung, J.-H. Lee, K.L. Beers, C.M. Stafford, Stiffness, strength, and ductility of nanoscale thin films and membranes: A combined wrinkling–cracking methodology. Nano Lett. **11**(8), 3361–3365 (2011)
70. J.Y. Chung, A.J. Nolte, C.M. Stafford, Diffusion-controlled, self-organized growth of symmetric wrinkling patterns. Adv. Mater. **21**(13), 1358–1362 (2009)
71. E.P. Chan, E.J. Smith, R.C. Hayward, A.J. Crosby, Surface wrinkles for smart adhesion. Adv. Mater. **20**(4), 711–716 (2008)
72. D. Breid, A.J. Crosby, Surface wrinkling behavior of finite circular plates. Soft Matter **5**(2), 425–431 (2009)
73. H. Vandeparre, P. Damman, Wrinkling of stimuloresponsive surfaces: Mechanical instability coupled to diffusion. Phys. Rev. Lett. **101**(12), 124301 (2008)
74. H. Vandeparre, J. Léopoldès, C. Poulard, S. Desprez, G. Derue, C. Gay, P. Damman, Slippery or sticky boundary conditions: Control of wrinkling in metal-capped thin polymer films by selective adhesion to substrates. Phys. Rev. Lett. **99**(18), 188302 (2007)
75. S.K. Basu, A.V. McCormick, L.E. Scriven, Stress generation by solvent absorption and wrinkling of a cross-linked coating atop a viscous or elastic base. Langmuir **22**(13), 5916–5924 (2006)
76. H.S. Kim, A.J. Crosby, Solvent-responsive surface via wrinkling instability. Adv. Mater. **23**(36), 4188–4192 (2011)

77. M. Guvendiren, S. Yang, J.A. Burdick, Swelling-induced surface patterns in hydrogels with gradient crosslinking density. Adv. Funct. Mater. **19**(19), 3038–3045 (2009)
78. M. Guvendiren, J.A. Burdick, S. Yang, Kinetic study of swelling-induced surface pattern formation and ordering in hydrogel films with depth-wise crosslinking gradient. Soft Matter **6**(9), 2044–2049 (2010)
79. S. Basu, L.E. Scriven, L.F. Francis, A.V. McCormick, Mechanism of wrinkle formation in curing coatings. Prog. Org. Coat. **53**(1), 1–16 (2005)
80. S. Yang, K. Khare, P.-C. Lin, Harnessing surface wrinkle patterns in soft matter. Adv. Funct. Mater. **20**(16), 2550–2564 (2010)
81. D. Chandra, A.J. Crosby, Self-wrinkling of UV-cured polymer films. Adv. Mater. **23**(30), 3441–3445 (2011)
82. Y. Li, J.J. Peterson, S.B. Jhaveri, K.R. Carter, Patterned polymer films via reactive Silane infusion-induced wrinkling. Langmuir **29**(14), 4632–4639 (2013)
83. S. Basu, L.E. Scriven, L.F. Francis, A.V. McCormick, V. Reichert, Wrinkling of epoxy powder coatings. J. Appl. Polym. Sci. **98**(1), 116–129 (2005)
84. J.M. Torres, C.M. Stafford, B.D. Vogt, Photoinitator surface segregation induced instabilities from polymerization of a liquid coating on a rigid substrate. Soft Matter **8**(19), 5225–5232 (2012)
85. Y. Gan, X. Jiang, J. Yin, Self-wrinkling patterned surface of photocuring coating induced by the fluorinated POSS containing thiol groups (F-POSS-SH) as the reactive Nanoadditive. Macromolecules **45**(18), 7520–7526 (2012)
86. R. Schubert, T. Scherzer, M. Hinkefuss, B. Marquardt, J. Vogel, M.R. Buchmeiser, VUV-induced micro-folding of acrylate-based coatings. 1. Real-time methods for the determination of the micro-folding kinetics. Surf. Coat. Technol. **203**(13), 1844–1849 (2009)
87. T. Tanaka, S.T. Sun, Y. Hirokawa, S. Katayama, J. Kucera, Y. Hirose, T. Amiya, Mechanical instability of gels at the phase-transition. Nature **325**(6107), 796–798 (1987)
88. E.S. Matsuo, T. Tanaka, Patterns in shrinking gels. Nature **358**(6386), 482–485 (1992)
89. T. Mizoue, Y. Aoki, M. Tokita, H. Honjo, H.J. Barraza, H. Katsuragi, Control of polymer gel surface pattern formation and its three dimensional measurement method. J. Polym. Eng. **30**(9), 523–534 (2010)
90. T. Mizoue, M. Tokita, H. Honjo, H.J. Barraza, H. Katsuragi, The effective surface roughness scaling of the gelation surface pattern formation, in *Gels: Structures, Properties, and Functions: Fundamentals and Applications*, ed. by M. Tokita, K. Nishinari (Springer, Berlin, 2009), pp. 63–67
91. M. Tokita, S. Suzuki, K. Miyamoto, T. Komai, Confocal laser scanning microscope imaging of a pattern in shrinking gel. J. Phys. Soc. Jpn. **68**(2), 330–333 (1999)
92. M. Tokita, K. Miyamoto, T. Komai, Polymer network dynamics in shrinking patterns of gels. J. Chem. Phys. **113**(4), 1647–1650 (2000)
93. E.P. Chan, E.J. Smith, R.C. Hayward, A.J. Crosby, Surface wrinkles for smart adhesion. Adv. Mater. **20**(4), 711 (2008)
94. K. Huraux, T. Narita, B. Bresson, C. Frétigny, F. Lequeux, Wrinkling of a nanometric glassy skin/crust induced by drying in poly (vinyl alcohol) gels. Soft Matter **8**(31), 8075–8081 (2012)
95. B. Li, Y.-P. Cao, X.-Q. Feng, H. Gao, Mechanics of morphological instabilities and surface wrinkling in soft materials: A review. Soft Matter **8**(21), 5728–5745 (2012)
96. E.S. Matsuo, T. Tanaka, Patterns in shrinking gels. Nature **358**(6386), 482 (1992)
97. L. Pauchard, C. Allain, Stable and unstable surface evolution during the drying of a polymer solution drop. Phys. Rev. E **68**(5), 052801 (2003)
98. L. Pauchard, C. Allain, Buckling instability induced by polymer solution drying. Europhys. Lett. **62**(6), 897–903 (2003)
99. R. Rizzieri, L. Mahadevan, A. Vaziri, A. Donald, Superficial wrinkles in stretched, drying gelatin films. Langmuir **22**(8), 3622–3626 (2006)

100. J.M. Katzenstein, D.W. Janes, J.D. Cushen, N.B. Hira, D.L. McGuffin, N.A. Prisco, C.J. Ellison, Patterning by photochemically directing the Marangoni effect. ACS Macro Lett. **1**(10), 1150–1154 (2012)
101. A.R. Jones, C.B. Kim, S.X. Zhou, H. Ha, R. Katsumata, G. Blachut, R.T. Bonnecaze, C.J. Ellison, Generating large thermally stable Marangoni-driven topography in polymer films by stabilizing the surface energy gradient. Macromolecules **50**(11), 4588–4596 (2017)
102. B.K. Chae, D.W. Janes, D.L. McGuffin, C.J. Ellison, Surface energy gradient driven convection for generating nanoscale and microscale patterned polymer films using photosensitizers. J. Polym. Sci. B Polym. Phys. **52**(18), 1195–1202 (2014)
103. A. Lasagni, C. Holzapfel, F. Mücklich, Periodic pattern formation of intermetallic phases with long range order by laser interference metallurgy. Adv. Eng. Mater. **7**(6), 487–492 (2005)
104. F. Mücklich, A. Lasagni, C. Daniel, Laser interference metallurgy—Periodic surface patterning and formation of intermetallics. Intermetallics **13**(3–4), 437–442 (2005)
105. A.F. Lasagni, D.F. Acevedo, C.A. Barbero, F. Mücklich, One-step production of organized surface architectures on polymeric materials by direct laser interference patterning. Adv. Eng. Mater. **9**(1–2), 99–103 (2007)
106. F. Yu, P. Li, H. Shen, S. Mathur, C.-M. Lehr, U. Bakowsky, F. Mücklich, Laser interference lithography as a new and efficient technique for micropatterning of biopolymer surface. Biomaterials **26**(15), 2307–2312 (2005)
107. D.A. Acevedo, A.F. Lasagni, C.A. Barbero, F. Mücklich, Simple fabrication method of conductive polymeric arrays by using direct laser interference micro-/Nanopatterning. Adv. Mater. **19**(9), 1272–1275 (2007)
108. A. Lasagni, D. Acevedo, C. Barbero, F. Mücklich, Advanced design of conductive polymeric arrays with controlled electrical resistance using direct laser interference patterning. Appl. Phys. A **91**(3), 369–373 (2008)
109. A.F. Lasagni, J.L. Hendricks, C.M. Shaw, D. Yuan, D.C. Martin, S. Das, Direct laser interference patterning of poly (3, 4-ethylene dioxythiophene)-poly (styrene sulfonate)(PEDOT-PSS) thin films. Appl. Surf. Sci. **255**(22), 9186–9192 (2009)
110. A. Lasagni, D. Acevedo, C. Barbero, F. Mücklich, Direct patterning of polystyrene–polymethyl methacrylate copolymer by means of laser interference lithography using UV laser irradiation. Polym. Eng. Sci. **48**(12), 2367–2372 (2008)
111. E. Rebollar, S. Pérez, J.J. Hernández, I. Martín-Fabiani, D.R. Rueda, T.A. Ezquerra, M. Castillejo, Assessment and formation mechanism of laser-induced periodic surface structures on polymer spin-coated films in real and reciprocal space. Langmuir **27**(9), 5596–5606 (2011)
112. E. Rebollar, D.R. Rueda, I. Martín-Fabiani, Á. Rodríguez-Rodríguez, M.-C. García-Gutiérrez, G. Portale, M. Castillejo, T.A. Ezquerra, In situ monitoring of laser-induced periodic surface structures formation on polymer films by grazing incidence small-angle X-ray scattering. Langmuir **31**(13), 3973–3981 (2015)
113. Á. Rodríguez-Rodríguez, E. Rebollar, M. Soccio, T.A. Ezquerra, D.R. Rueda, J.V. Garcia-Ramos, M. Castillejo, M.-C. Garcia-Gutierrez, Laser-induced periodic surface structures on conjugated polymers: Poly(3-hexylthiophene). Macromolecules **48**(12), 4024–4031 (2015)
114. I. Michaljaničová, P. Slepička, S. Rimpelová, N. Slepičková Kasálková, V. Švorčík, Regular pattern formation on surface of aromatic polymers and its cytocompatibility. Appl. Surf. Sci. **370**, 131–141 (2016)
115. Z. Guosheng, P. Fauchet, A. Siegman, Growth of spontaneous periodic surface structures on solids during laser illumination. Phys. Rev. B **26**(10), 5366 (1982)
116. A. Barborica, I. Mihailescu, V. Teodorescu, Dynamical evolution of the surface microrelief under multiple-pulse-laser irradiation: An analysis based on surface-scattered waves. Phys. Rev. B **49**(12), 8385 (1994)
117. S. Baudach, J. Bonse, W. Kautek, Ablation experiments on polyimide with femtosecond laser pulses. Appl. Phys. A **69**(1), S395–S398 (1999)

118. S. Baudach, J. Krüger, W. Kautek, Femtosecond laser processing of soft materials. Rev. Laser Eng. **29**(11), 705–709 (2001)
119. M. Forster, W. Kautek, N. Faure, E. Audouard, R. Stoian, Periodic nanoscale structures on polyimide surfaces generated by temporally tailored femtosecond laser pulses. Phys. Chem. Chem. Phys. **13**(9), 4155–4158 (2011)
120. W. Biegel, *D. Bliuerle Laser Processing and Chemistry* (Springer, Berlin/Heidelberg/New York, 1996). ISBN: 3-540-60541-X, DM 128, 00. Berichte der Bunsengesellschaft für physikalische Chemie **101**(6), 984–984 (1997)
121. E. Rebollar, J.R.V. de Aldana, I. Martín-Fabiani, M. Hernández, D.R. Rueda, T.A. Ezquerra, C. Domingo, P. Moreno, M. Castillejo, Assessment of femtosecond laser induced periodic surface structures on polymer films. Phys. Chem. Chem. Phys. **15**(27), 11287–11298 (2013)